Chapter 5. Heterogeneous Simulations

5.1 Introduction

In order for a numerical model to accurately predict subsurface transport and biodegradation, it must account for the physical variations within soils as well as the biological and chemical processes of contaminant decay. Thus, in recent years, research has focused on placing soil variability in a probabilistic framework, and a stochastic approach has been used to capture the effects of soil heterogeneity. The theory of stochastic flow and transport in the subsurface has been developed and reviewed by numerous authors (for example Gelhar, 1986; Jury et al., 1987; Dagan, 1990; Russo, 1991). Numerous studies have focused on water flow and dissolved phase transport in heterogeneous saturated and unsaturated soils (for example, Russo, 1991; Chen et al., 1994; Russo et al., 1994).

A limited number of researchers have examined the effect of soil heterogeneity on transport of biodegradable solutes. MacQuarrie and Sudicky (1990) studied transport of an organic substrate with oxygen as the sole electron acceptor (EA), and found that the most significant parameters were the initial concentrations of substrate and oxygen, the average groundwater velocity, the retardation factor, and the degree of heterogeneity in the porous medium. The rate of substrate mass loss was weakly dependent on initial biomass density and the kinetic biodegradation parameters. Overall, biodegradation had a significant effect on transport, and MacQuarrie and Sudicky recommended that the average transport parameters such as macrodispersivity may not apply to migration of a biodegradable plume. Miralles-Wilhelm et al. (1997) used a three-dimensional analytical model to perform a stochastic analysis of transport of a solute with oxygen-limited biodegradation. It was found that heterogeneities in aquifer permeability, the adsorption parameter, and the microbial kinetic parameters led to effective, field-scale decay rates that were significantly less than the mean decay rate. Therefore, computations based on the mean decay rate would overpredict the actual mass loss of contaminant.

The purpose of the present study was to use the three-dimensional sequential electron acceptor model (SEAM3D) to evaluate the effects of heterogeneities in soil and microbial parameters on the subsurface transport of a biodegradable solute using oxygen and sulfate as

EAs. The solute was conceptualized as an aromatic hydrocarbon with properties similar to toluene, and a nondegradable tracer was also simulated for comparison. A hypothetical slug of hydrocarbon and tracer was injected in a three-dimensional domain and the subsequent transport was examined using statistical and spatial moment analyses. The turning bands method (Mantoglou and Wilson, 1982) was used to generate porous media that represented hypothetical yet realistic sandy loam soils. The method was also used to generate heterogeneous fields of microbial populations. Stochastic input parameters for the flow model (MODFLOW) included the horizontal hydraulic conductivity (K_h) and the vertical leakance (V_{cont}), which is defined as the harmonic mean of the vertical hydraulic conductivity between adjacent blocks. For the transport and biodegradation model (SEAM3D), heterogeneous inputs included the maximum specific rate of substrate utilization ($\nu^{max}_{x,ls,le}$) and the initial biomass concentration (M_x).

5.2 Model Descriptions

5.2.1 Flow model

The governing equations and the finite difference solution for the flow model is described in the MODFLOW user manual (McDonald and Harbaugh, 1988). Therefore, this section is limited to definitions of the parameters that will be considered stochastic in the numerical experiments to follow. As input, MODFLOW requires the transmissivity (T) of all confined aquifer layers and the vertical leakance between layers. For a confined aquifer of layer thickness Δz_k , the transmissivity is defined as $T = K_h \Delta z_k$, where K_h is the horizontal saturated hydraulic conductivity. The vertical leakance ($V_{cont,\, k+1/2}$) is defined as the harmonic mean of the vertical hydraulic conductivity between adjacent blocks in models layers *k* and *k+1*, and is calculated as (McDonald and Harbaugh, 1988)

$$V_{cont,\, k+1/2} = \frac{1}{\dfrac{\Delta z_k / 2}{K_{z,\, k}} + \dfrac{\Delta z_{k+1} / 2}{K_{z,\, k+1}}} \tag{5.1}$$

where Δz_k is the thickness of model layer *k* and $K_{z,k}$ is the vertical hydraulic conductivity of layer *k*. Due to the nature of many geological deposits, the vertical component of hydraulic conductivity is often less than the horizontal component.

5.2.2 Biodegradation model

The biodegradation model (SEAM3D) used in these simulations is described fully in Chapter 2 of this work. Parameters that were allowed to be stochastic include the maximum specific rate of substrate utilization ($\nu_{x,ls,le}^{max}$) and the initial biomass concentration (M_x).

5.3 Methods of Analysis of Plume Behavior

5.3.1 Spatial Moments of the Solute Plumes

In order to evaluate the average, large scale movement of the solute plumes, the first and second spatial moments of the concentration distribution were calculated at five day intervals. At time t, the *ijk*th spatial moments of a solute with concentration C may be defined as (Aris, 1956)

$$M_{ijk}(t) = \int_{-\infty}^{\infty} \int_{-\infty}^{\infty} \int_{-\infty}^{\infty} \theta(x, y, z; t)\ C(x, y, z; t)\ x^i y^j z^k\ \partial x\ \partial y\ \partial z \qquad (5.2)$$

where θ is effective porosity. The zero order moment (M_{000}) provides an estimate of the total mass of solute in the domain, while the first order moments (M_{100}, M_{010}, and M_{001}) can be used to calculate the location of the center of mass (x_c, y_c, z_c) of the solute plume. These components of center of mass were computed as

$$x_c = M_{100} / M_{000} \qquad (5.3a)$$

$$y_c = M_{010} / M_{000.} \qquad (5.3b)$$

$$z_c = M_{001} / M_{000.} \qquad (5.3c)$$

The second order moments (M_{200}, M_{020}, and M_{002}) were used to compute the spatial standard deviations of the solute plume in the x-direction (σ_{xx}), the y-direction (σ_{yy}), and the z-direction (σ_{zz}), as

$$\sigma_{xx} = \sqrt{\frac{M_{200}}{M_{000}} - x_c^2} \qquad (5.4a)$$

$$\sigma_{yy} = \sqrt{\frac{M_{020}}{M_{000}} - y_c^2}\ . \qquad (5.4b)$$

$$\sigma_{zz} = \sqrt{\frac{M_{002}}{M_{000}} - z_c^2} \ . \tag{5.4c}$$

The spatial standard deviations indicate the average amount of solute spreading in the x, y, and z-directions.

The average velocity of the solute plume in the x-direction (v_x) at time t was calculated as

$$v_x = \frac{(x_c^t - x_c^{t-\Delta t})}{\Delta t} \tag{5.5}$$

where the time interval Δt was a constant 5 days. The average y and z-velocities (v_y and v_z) were computed in an analogous manner.

5.3.2 Statistical Analysis

The mean and the coefficients of variation (CVs) of the resident and flux hydrocarbon concentrations were calculated over time in the y-z plane at a specified x-location in the model domain. The mean resident concentration may be defined as the concentration averaged over a volume of the porous medium, while the mean flux concentration is the weighted average of small scale (in this case defined by a model block) concentrations using the individual model block velocities as the weighting factors (Parker and van Genuchten, 1984). At time *t* and location *x*, the mean resident concentration $\langle C_r(x;t) \rangle$ was calculated as

$$\langle C_r(x;t) \rangle = \frac{\int_{-\infty}^{\infty} \int_{-\infty}^{\infty} \theta(x,y,z;t)\ C(x,y,z;t)\ \partial y\ \partial z}{\int_{-\infty}^{\infty} \int_{-\infty}^{\infty} \theta(x,y,z;t)\ \partial y\ \partial z} \tag{5.6}$$

while the mean flux concentration $\langle C_f(x;t) \rangle$ was calculated as

$$\langle C_f(x;t) \rangle = \frac{\int_{-\infty}^{\infty} \int_{-\infty}^{\infty} q_n(x,y,z;t)\ C(x,y,z;t)\ \partial y\ \partial z}{\int_{-\infty}^{\infty} \int_{-\infty}^{\infty} q_n(x,y,z;t)\ \partial y\ \partial z} \tag{5.7}$$

where q_n is the component of the water flux normal to the y-z plane. The CV is a normalized measure of variability and is calculated as the standard deviation of a group of data divided by the mean. The resident standard deviation (σ_r) was computed as

$$\sigma_r(x;t) = \sqrt{\int_{-\infty}^{\infty} \int_{-\infty}^{\infty} \left[\frac{\theta(x,y,z;t)\ C(x,y,z;t)}{\theta_{avg}} - \langle C_r(x;t) \rangle \right]^2 \partial y\ \partial z} \qquad (5.8)$$

where θ_{avg} is the average effective porosity in the y-z plane at location x. Likewise, the flux-averaged standard deviation σ_f was computed as

$$\sigma_f(x;t) = \sqrt{\int_{-\infty}^{\infty} \int_{-\infty}^{\infty} \left[\frac{q_n(x,y,z;t)\ C(x,y,z;t)}{q_{avg}} - \langle C_f(x;t) \rangle \right]^2 \partial y\ \partial z} \qquad (5.9)$$

where q_{avg} is the average flux normal to the y-z plane at location x.

5.4 Model Domain, Parameters, and Boundary Conditions

5.4.1 Grid spacing and control parameters

The three-dimensional model domain for flow and transport (Figure 5.1), was 40.5 m in the longitudinal x-direction, 20 m in the transverse y-direction, and 3 m in the vertical z-direction. In Figure 5.1 and all subsequent figures, the location z = 3 corresponds to model layer 1. The domain was divided into 40 rows, 81 columns, and 60 layers to generate 194,400 blocks of dimension 0.5 x 0.5 x 0.05 m. The entire aquifer was specified as confined, with uniform vertical thickness in each layer. The flow solution was steady state, while the transport simulations were transient with the transport time step set to 0.5 days and the biodegradation time step set to 0.25 days. Model simulations ran for 2000 days, taking approximately 8 hours of computational time on a Pentium Pro 200n personal computer with 64 megabytes RAM.

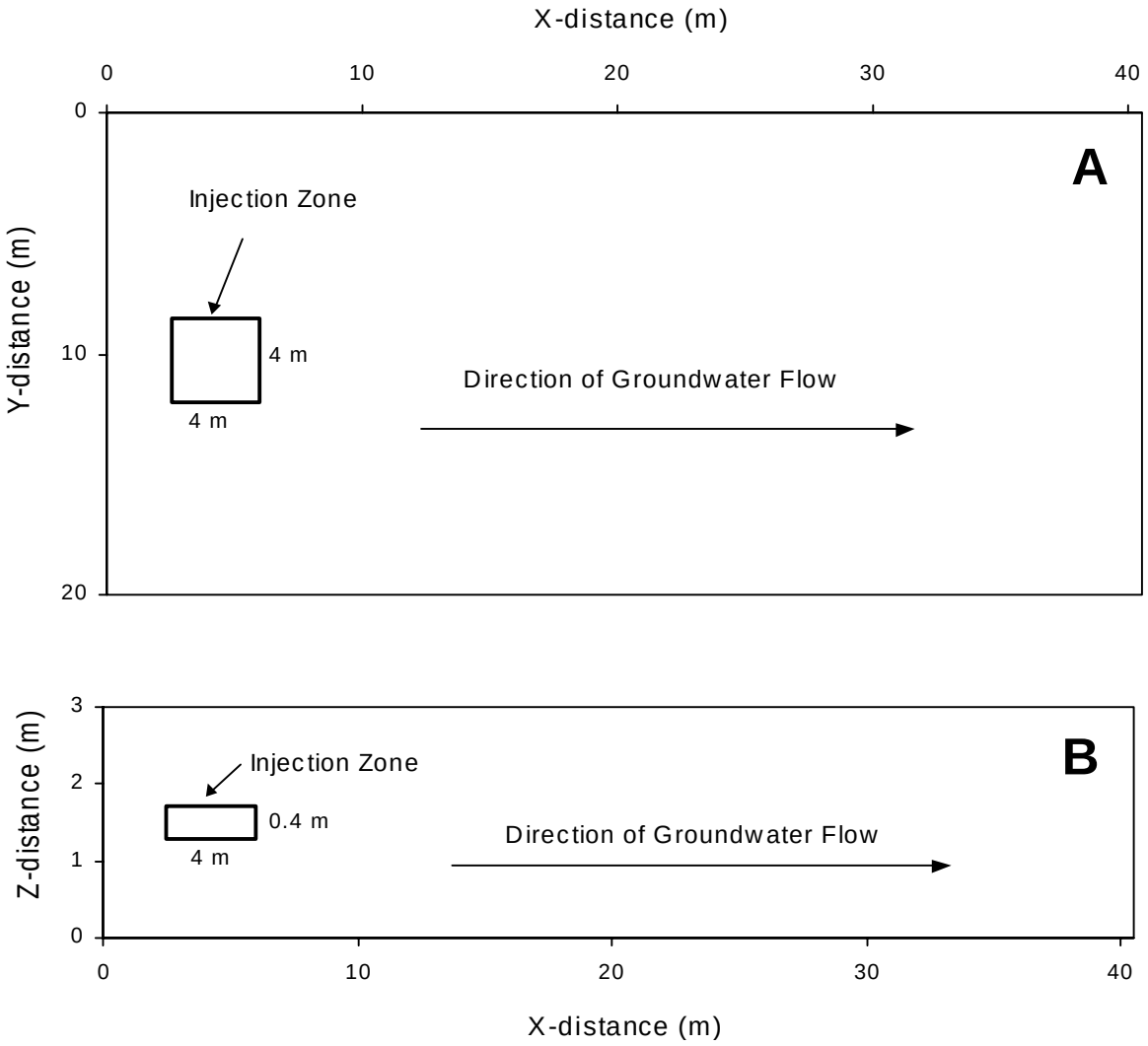

Figure 5.1. The three-dimensional model domain in an areal view (A) and in vertical cross section (B). Vertical scale is exaggerated.

5.4.2 Flow parameters and boundary conditions

The groundwater flow model MODFLOW (McDonald and Harbaugh, 1988) was used to generate the steady state flow field for contaminant transport. The horizontal hydraulic conductivity (K_h) was treated as a stochastic field variable, with values of K_h generated by the turning bands method (see Section 5.4.5 below). For every model layer *k*, each value in the horizontal hydraulic conductivity (K_h) field was multiplied by the thickness of the layer (Δz_k) to obtain the MODFLOW input values for transmissivity. In these simulations, Δz_k was a constant 0.05 m.

The boundary condition for hydraulic head was maintained at a constant value of 5.0 m at x = 0 and 4.9 m at x = 81. The top (z = 3) and bottom (z = 0) boundaries and the side boundaries (y = 0 and y = 20) were specified as no flow. Thus the average horizontal gradient in hydraulic head was 0.25% sloping from left to right in Figure 5.1, but variations in conductivity produced local irregularities in the flow field. It was assumed that K_h was two times greater than the K_v, and since Δz_k was a constant 0.05 m, the average value of V_{cont} was 10 m day^{-1}. Individual values of K_v were derived from the K_h field, so V_{cont} was spatially variable.

5.4.3 Transport parameters and boundary conditions

A contaminant leak was simulated as occurring instantaneously in the 4 x 4 x 0.4 m block shown in Figure 5.1. The contaminant was conceptualized as containing a biodegradable hydrocarbon and a nonbiodegradable tracer. In all but one case, the model domain was allowed to contain the electron acceptors (EAs) oxygen and sulfate, and the product H_2S was produced during sulfate reduction. Additional EA processes were omitted in order to conserve computer memory and maximize the number of model blocks in the simulation. In order to examine the effect of sulfate on the biodegradation process, a simulation was made using oxygen as the sole EA. Values for the longitudinal dispersivity (α_x), transverse dispersivity (α_y), vertical dispersivity (α_z), effective porosity (θ), and soil bulk density (ρ_b) were constant over the entire domain (Table 5.1). Dispersivities were chosen to be quite small, based on the laboratory scale dimensions of the individual model blocks. The soil bulk density was chosen as typical of a

sandy soil (Carsel and Parrish, 1988). None of the aqueous phase components were allowed to adsorb to the soil, so the retardation factor was equal to one for all components. Based on the value of 0.35 for θ, the average groundwater velocity was approximately 0.0071 m day^{-1}, although individual block velocities varied with the distribution of K_h.

In all cases, initial concentrations were zero everywhere for H_2S, and zero in all locations outside the injection zone (Figure 5.1) for the hydrocarbon and tracer. For the base case, the initial concentrations were 3.0 g m^{-3} for oxygen and 30.0 g m^{-3} for sulfate in all locations, and 60 g m^{-3} for the hydrocarbon and tracer in the zone of injection. In order to simulate the instantaneous injection, the boundary condition was set as constant concentration for a single time step within the injection zone. Afterwards these blocks became active, such that concentration varied according to the model solution, and contaminant mass was no longer added to the domain. Boundary conditions were specified as constant concentration equal to the initial condition at x = 0 for all aqueous phase constituents. All other blocks were allowed to be active, with variable concentrations. If a solute reached the outflow boundary of the domain at x = 41 m, solute mass was allowed to exit under a zero dispersion boundary condition.

Table 5.1. Transport parameters representing longitudinal dispersivity (α_x), transverse dispersivity (α_y), vertical dispersivity (α_z), effective porosity (θ), and soil bulk density (ρ_b).

α_x	α_y	α_z	θ	ρ_b
(m)	(m)	(m)	(-)	($g\ m^{-3}$)
0.01	0.001	0.0001	0.35	1.6×10^6

5.4.4 Biodegradation parameters

For the base case, model parameters for biodegradation (Table 5.2) were constant in space for both the aerobes and the sulfate reducers. In order to reflect the high rate and energy yield of aerobic metabolism, parameters controlling aerobic utilization, growth, and death were higher than those of the anaerobic, sulfate reducing process. Biodegradation parameters were based on typical values reported in the literature. For aerobic biodegradation of hydrocarbons, laboratory estimates of $\nu^{max}_{x,ls,le}$ have been reported as 1.0 day^{-1} (Kindred and Celia, 1989), 1.7 day^{-1} (Borden and Bedient, 1986), 3.5 to 8.0 day^{-1} (Arcangeli and Arvin, 1992), and 8.3 to 9.9 day^{-1} (Chen et al., 1992). Biodegradation rates in the field may be much lower than observed in the laboratory, as Chapelle and Lovley (1990) have reported that microbial metabolic rates based on laboratory incubations may overpredict in situ rates by two orders of magnitude. For hydrocarbons, the half saturation coefficient $K^{s}_{x,ls,le}$ has been reported to vary widely as 0.1 g m^{-3} (Kindred and Celia, 1989), 0.13 g m^{-3} (Borden and Bedient, 1986), 0.6 g m^{-3} (Arcangeli and Arvin, 1992), 1.88 to 4.55 g m^{-3} (Chang et al., 1993), and 12.2 to 17.4 g m^{-3} (Chen et al., 1992). For oxygen, $K^{e}_{x,le}$ has been reported as 0.10 g m^{-3} (Borden and Bedient, 1986; Kindred and Celia, 1989; Chen et al., 1992). The yield coefficient ($Y_{x,ls,le}$) for aerobes is often estimated as 0.5 g g^{-1} (Arcangeli and Arvin, 1992; Borden and Bedient, 1986; Chen et al., 1992; Wodzinski and Johnson, 1968). For anaerobes, $Y_{x,ls,le}$ is usually lower than for aerobes, with 0.2 g g^{-1} being the theoretical maximum yield under sulfate reducing conditions (Edwards et al., 1992). The effective death terms ($k^{bk}_{d_x}$) were calculated internally by SEAM3D, using the method described in Section 2.1.4.

For inhibition by oxygen, $\kappa_{le,li}$ values have been reported to vary between 0.01 and 0.1 g m^{-3} (Kindred and Celia, 1989; Chen et al., 1992). EA use coefficients ($\gamma_{x,ls,le}$) were estimated from the stoichiometric relationship between each EA and the corresponding hydrocarbon, using toluene as a representative compound. Thus, values for $\gamma_{x,ls,le}$ were 3.2 g g^{-1} for O_2, and 4.5 g g^{-1} for SO_4^{2-} (Borden et al., 1995). The H_2S generation term ($\zeta_{x,le}$) of 0.8 g g^{-1} was also based on stoichiometric relationships (Edwards et al., 1992). In all cases the initial microbial biomass (M_x) was higher for the aerobes than the sulfate reducers, based on the assumption that aerobic

biomass would predominate when the groundwater contained significant O_2 under pristine conditions. Thus, the biomass concentration of sulfate reducers was an order of magnitude lower than the aerobic biomass (Table 5.2). Threshold concentrations, below which biodegradation will not occur, were set to zero for all components.

Table 5.2. Electron acceptor (EA) initial concentrations and biodegradation parameters representing maximum specific rate of substrate utilization ($\nu^{max}_{x,ls,le}$), substrate half saturation constant ($K^{s}_{x,ls,le}$), EA half saturation constant ($K^{e}_{x,le}$), yield coefficient ($Y_{x,ls,le}$), EA use coefficient ($\gamma_{x,ls,le}$), inhibition coefficient ($\kappa_{le,li}$), generation coefficient ($\zeta_{x,li}$), initial biomass concentration (M_x), and background death rate ($k^{bk}_{d_x}$) for each microbial population. These parameters represent the base case simulation.

Microcolony / EA	$\nu^{max}_{x,ls,le}$	$K^{s}_{x,ls,le}$	$K^{e}_{x,le}$	$Y_{x,ls,le}$	$\gamma_{x,ls,le}$	$\kappa_{le,li}$	$\zeta_{x,li}$	M_x	$k^{bk}_{d_x}$
	(day^{-1})	($g\ m^{-3}$)	($g\ m^{-3}$)	($g\ g^{-1}$)	($g\ g^{-1}$)	($g\ m^{-3}$)	($g\ g^{-1}$)	($g\ m^{-3}$)	(day^{-1})
Aerobes / O_2	1.0	5.0	0.5	0.5	3.2	0.1	--	0.10	0.43
Sulfate reducers / SO_4	0.1	5.0	0.5	0.2	4.5	--	0.8	0.01	0.020

5.4.5 Generation of stochastic parameters

In all cases, the geometric mean soil parameters were characteristic of a sandy loam (Carsel and Parrish, 1988). The porosity was chosen to be a constant 0.40 because the variability in porosity for a particular soil is generally small. As called for in the various model simulation cases (Table 5.3), the horizontal hydraulic conductivity (K_h), the maximum specific rate of substrate utilization ($\nu^{max}_{x,ls,le}$), and the initial biomass concentrations (M_x) were assumed to be lognormally distributed, locally stationary, random space variables described by the following three dimensional, anisotropic covariance function:

$$C(s_x, s_y, s_z) = \sigma^2_{ln(i)} \exp\left[-\sqrt{\left(\frac{s_x^2}{\eta_x^2} + \frac{s_y^2}{\eta_y^2} + \frac{s_z^2}{\eta_z^2}\right)}\right] \tag{5.10}$$

where s_x, s_y, and s_z are the separation (or lag) distances in the x, y, and z-directions, η is the correlation scale based on the e^{-1} criterion, and $\sigma^2_{ln(i)}$ is the variance of ln(i) for i = K_h, $\nu^{max}_{x,ls,le}$, or M_x. The turning bands method (Mantoglou and Wilson, 1982) as implemented by Tompson et al. (1987) was used to produce the random, statistically homogeneous fields of soil properties. The program requires input values for the geometric mean and the standard deviation (σ) of the natural log-transformed field variable (i.e., K_h, $\nu^{max}_{x,ls,le}$, or M_x). Also required are the number of nodes, the nodal spacing, and the correlation scales of the field variable in the x, y, and z directions. The output of the turning bands program is a value of K_h, $\nu^{max}_{x,ls,le}$, or M_x at each node of the model domain. Thus, for MODFLOW, a distinct value for K_h was used to calculate transmissivity for each of the 194,400 nodes in the domain. The K_h field was also used to calculate V_{cont} (equation 5.1), under the assumption that K_z = 0.5 K_h. The spatial autocorrelation among K_h values for the base case realization (Figure 5.2) corresponds closely to the theoretical values from equation 5.11. A similar correspondence was observed (data not shown) for the other realizations.

The actual values for K_h in the base case vary over several orders of magnitude (Table 5.3), but due to autocorrelation, the ratio in K_h for any two adjacent nodes rarely exceeded 6:1 for the base case. Autocorrelation produces observable zones of high and low values in the areal spatial distribution of K_h (Figure 5.3). Since the vertical correlation scale (0.15 m) is

greater than the separation distance (0.1 m) between layers 1 and 3, there is general correspondence between areas of high and low K_h for these layers. However, layer 30 shows no correspondence with layer 1 or 3 since the separation distance is much greater than the correlation scale.

Values for σ and η for K_h were based on published data, and the base case (Table 5.3) was chosen to be the most representative of a highly heterogeneous sandy loam. Jury et al. (1987) surveyed the literature on the spatial variability of K_h and found that $\sigma_{\ln K_h}$ ranged from 0.5 to 1.6, but only two of the thirteen values exceeded 1.2. Gelhar (1986) found that $\sigma_{\ln K_h}$ was less than or equal to 1.0 in 10 of 13 studies of soils or aquifers. Thus, $\sigma_{\ln K_h}$ = 1.0 was chosen to represent a relatively high degree of variability in K_h for the base case.

In order for a discretized model domain to capture spatial correlation, Ababou (1988) suggests using at least four nodes per correlation scale (η). To satisfy the ergodic hypothesis, it is recommended that the flow domain extend over a large number of correlation scales. Thus, the spatially averaged soil properties from a single realization may be expected to correspond to the ensemble mean taken over a large number of realizations (Dagan, 1990; Gelhar, 1986). In at least two field studies, the variability in hydraulic conductivity has been measured in sufficient detail to compare the correlation scales in the horizontal and vertical directions. At the Borden site in Canada, Sudicky (1986) estimated that $\eta_x = \eta_y = 2.8$ m and $\eta_z = 0.12$ m. In the New Mexico Sevilleta Wildlife Refuge, Byers and Stephans (1983) found that $\eta_x = \eta_y = 0.6$ m and $\eta_z = 0.08$ m. Based on the above criteria, η_x and η_y were chosen as 1.5 m for the base case (Table 5.3), and η_y remained equal to η_x in all subsequent cases. Since the vertical correlation scale is generally much smaller than the horizontal, the vertical correlation scale (η_z) was set equal to $0.1\eta_x$ in all cases.

Alternative model scenarios were simulated to examine the influence of the stochastic parameters and the degree of heterogeneity on model output (Table 5.3). For the flow model, the effect of the standard deviation of K_h ($\sigma_{\ln K_h}$) was examined in Case 2, while the effect of the correlation scale (η) was examined in Case 3 (Table 5.3). For Case 3a, η is given the same value as the block dimension, essentially allowing the values of K_h to be randomly distributed over the domain. In Case 4, the microbial parameters representing the maximum specific rate of

substrate utilization ($\nu^{max}_{x,ls,le}$) and the initial biomass concentration (M_x) were also allowed to be stochastic. The yield coefficients ($Y_{x,ls,le}$), the EA use coefficients ($\gamma_{x,ls,le}$), and the EA generation term ($\zeta_{x,ls}$) were not considered as stochastic since it was assumed that they could be estimated with reasonable accuracy from stoichiometric relationships. Since there is limited information in the literature on the subsurface distributions of $\nu^{max}_{x,ls,le}$ and M_x, it was assumed that $\sigma_i = 0.5$ and $\eta_i = 1.5$ m for i = $\nu^{max}_{x,ls,le}$ and M_x. These values produced random fields with reasonable ranges of values for $\nu^{max}_{x,ls,le}$ and M_x (Table 5.3).

In the literature there are numerous reports of a positive correlation between hydraulic conductivity and microbial activity. In a review of the literature, Thomas and Ward (1992) concluded that microbial activity is higher in high permeability sand layers than in low conductivity aquitards. In deep, anaerobic coastal plain aquifers, Chapelle and Lovely (1990) found that microbial metabolic rates were greater in sandy sediments than clay layers. In shallow coastal plain sediments, Aelion and Long (1994) found that contaminated sand sediments had greater microbial activity than contaminated clay sediments. Konopka and Turco (1991) studied 17 soil samples taken from various depths in a 26 m borehole, and found that microbial activity was highest in the "transmissive layers." In contrast, Keift et al. (1995) found that coarse textured sands had lower microbial biomass concentrations and activities than fine-textured sediments at the Hanford site in Washington. Thus the parameters K_h, $\nu^{max}_{x,ls,le}$, and M_x were allowed to be correlated in Case 4a, while in Case 4b, they were uncorrelated. Correlation was produced by using the same initial seed number for the random number generator in the turning bands procedure to produce the random fields of K_h, $\nu^{max}_{x,ls,le}$, and M_x. Uncorrelated fields were produced by varying the initial seed number.

Table 5.3. Geometric means and the range of values for stochastic parameters representing the horizontal hydraulic conductivity (K_h), the maximum specific rate of substrate utilization ($\nu^{max}_{x,ls,le}$), and the initial biomass concentration (M_x). In each case, $\eta_x = \eta_y$ and $\eta_z = 0.1\eta_x$.

	Stochastic Parameter *i*	Standard Deviation $\sigma_{ln(i)}$	Correlation Scale η_x (m)	Geometric Mean	Minimum Value	Maximum Value
Base Case	K_h (m day^{-1})	1.0	1.5	1.0	0.011	66.6
Case 2a	K_h (m day^{-1})	0.5	1.5	1.0	0.106	8.16
Case 2b	K_h (m day^{-1})	1.25	1.5	1.0	0.0037	190.3
Case 3a	K_h (m day^{-1})	1.0	0.5	1.0	0.0069	84.7
Case 3b	K_h (m day^{-1})	1.0	3.0	1.0	0.0076	82.7
Case 4a	K_h (m day^{-1})	1.0	1.5	1.0	0.011	66.6
	$\nu^{max}_{1,ls,1}$ (day^{-1})	0.5	1.5	1.0	0.106	8.16
	$\nu^{max}_{2,ls,2}$ (day^{-1})	0.5	1.5	0.1	0.011	0.82
	M_1 (g m^{-3})	0.5	1.5	0.10	0.011	0.82
	M_2 (g m^{-3})	0.5	1.5	0.01	0.0011	0.082
Case 4b	K_h (m day^{-1})	1.0	0.5	1.0	0.011	66.6
	$\nu^{max}_{1,ls,1}$ (day^{-1})	0.5	1.5	1.0	0.116	9.11
	$\nu^{max}_{2,ls,2}$ (day^{-1})	0.5	1.5	0.1	0.010	0.91
	M_1 (g m^{-3})	0.5	1.5	0.10	0.013	0.85
	M_2 (g m^{-3})	0.5	1.5	0.01	0.0011	0.089

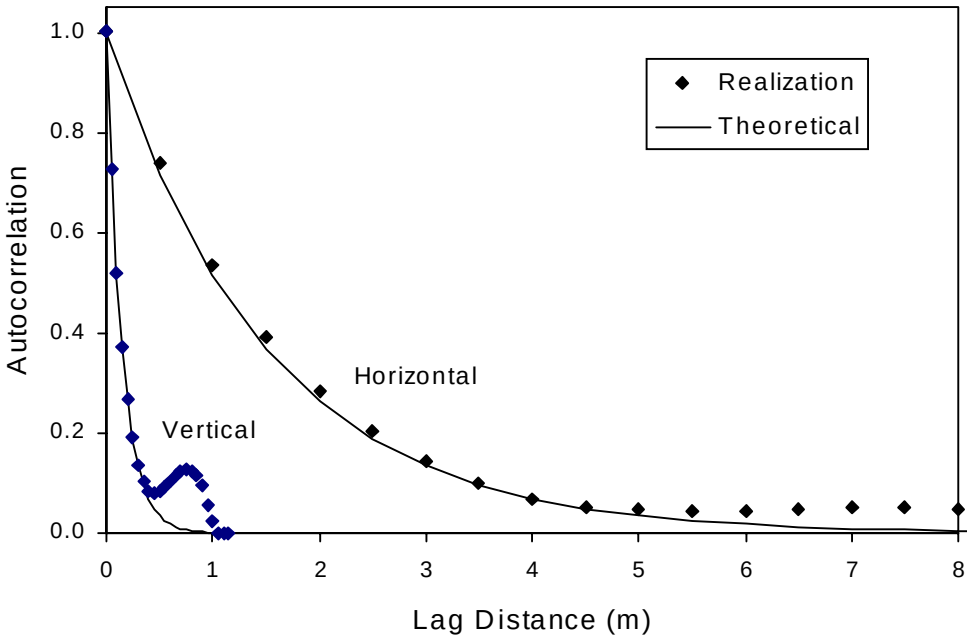

Figure 5.2. Autocorrelation of $\ln K_h$ in the x and z-directions for the base case. Values of the realization were produced by the turning bands method, and theoretical values were obtained from equation (5.11).

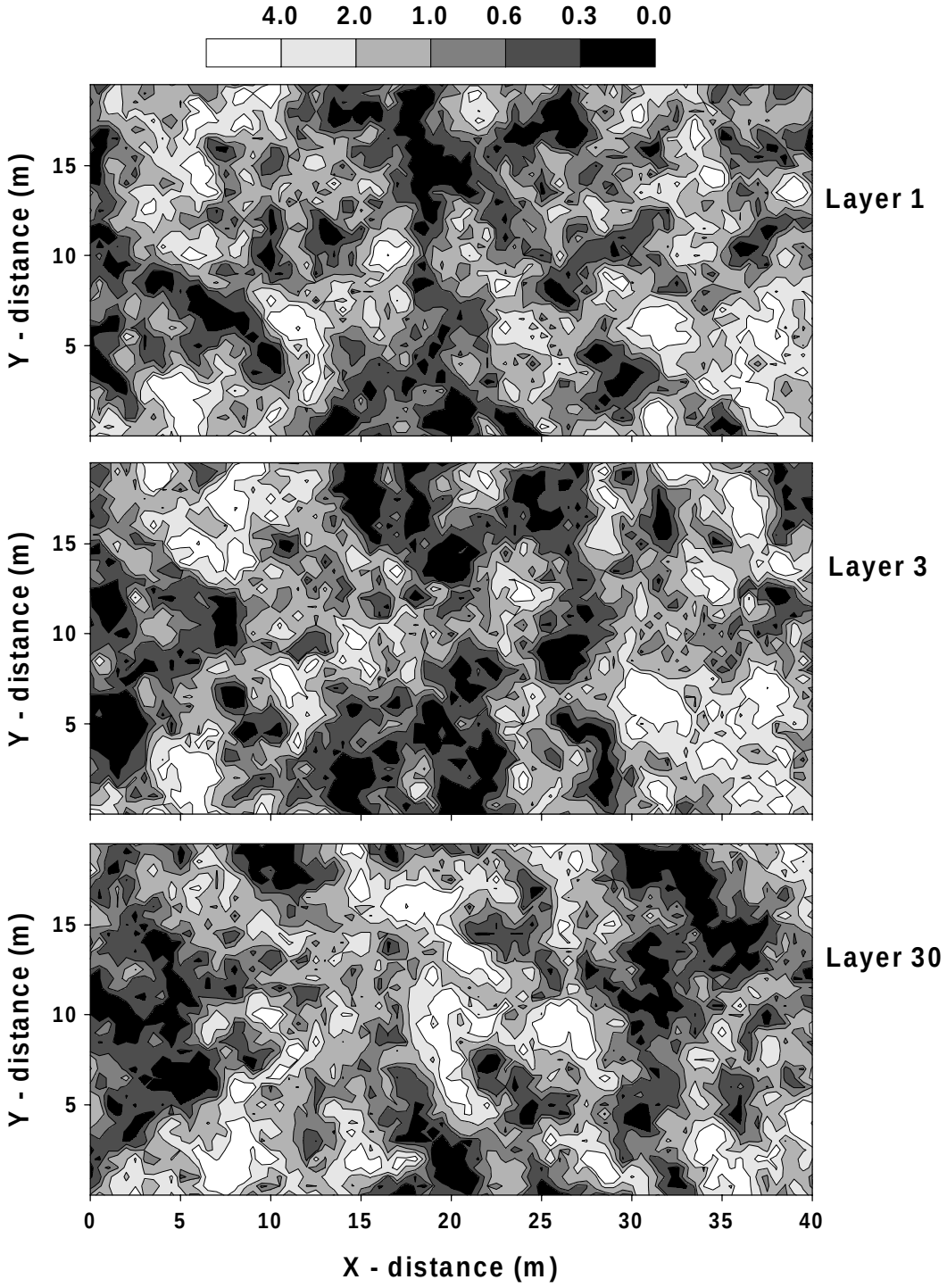

Figure 5.3. Filled contour intervals for the base case heterogeneous distribution of K_h in model layer 1, layer 3, and layer 30. Dimensions of the scale bar are m day^{-1}.

5.5 Transport Analysis

5.5.1 Base case plume migration

In order to illustrate plume migration through the 3-dimensional domain, base case model results are presented for a horizontal slice (layer 30) and a vertical slice (row 21) through the center of the domain. Biodegradation limits spreading in all directions, so the hydrocarbon plume is more compact than the tracer (Figure 5.4). In addition, biodegradation attenuates the maximum hydrocarbon concentration, which exceeds 3.0 g m^{-3} only in a small portion of the domain near x = 11 and z = 1.8. In contrast, the tracer concentration exceeds 3.0 g m^{-3} over large portions of the domain, and the maximum tracer concentration is greater than 6.0 g m^{-3}. By 2000 days, the downgradient edge of the tracer plume has reached the boundary, and mass begins to exit the domain (Figure 5.4).

The highest concentrations of hydrocarbon remain where oxygen has been depleted (Figure 5.5). These zones also correspond to the locations of maximum sulfate utilization, since the presence of oxygen inhibits sulfate reduction in other areas. The sulfate concentration drops below 10.0 g m^{-3} in only a small portion of the domain, indicating that biodegradation is being limited by the slow rate of utilization rather than the exhaustion of sulfate. The time evolution of sulfide (H_2S) at 500, 1000, and 1500 days (Figure 5.6) reveals that the maximum H_2S concentration does not increase with time, even though the area having H_2S increases. In fact the maximum H_2S concentration of 24.4 g m^{-3} is observed at 500 days. This suggests that the rate of sulfate reduction is decreasing as the concentration of hydrocarbon diminishes over time.

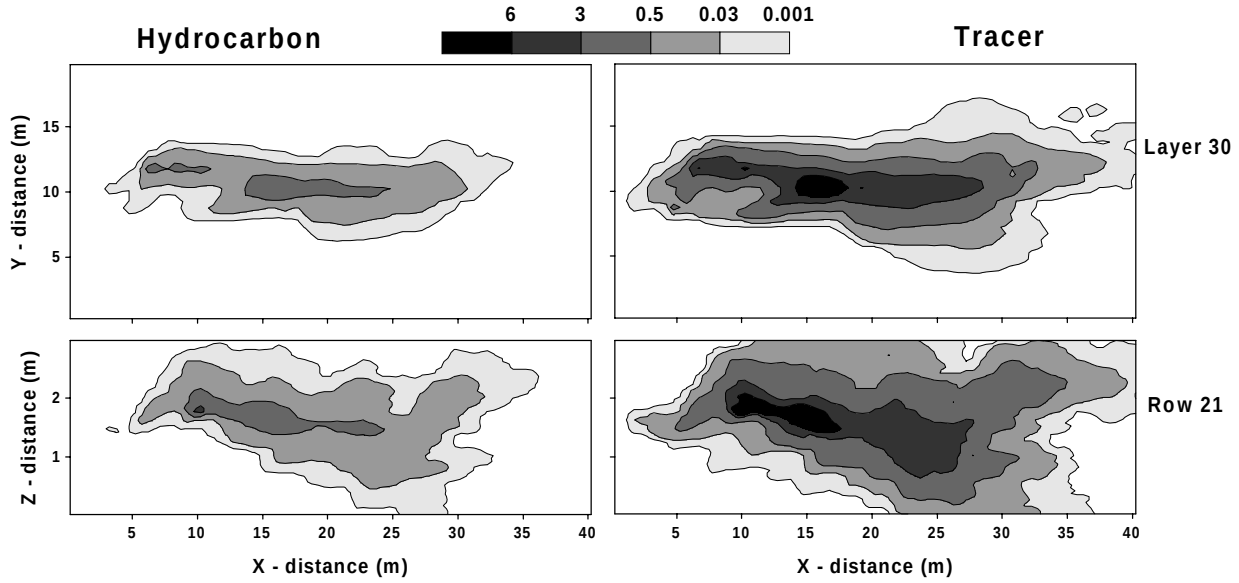

Figure 5.4. Distribution of biodegradable hydrocarbon and nondegradable tracer in a horizontal slice (layer 30) and a vertical slice (row 21) through the center of the model domain at 2000 days. The scale bar applies to all four figures, with dimensions of g m^{-3}. Vertical (z-direction) scale is exaggerated.

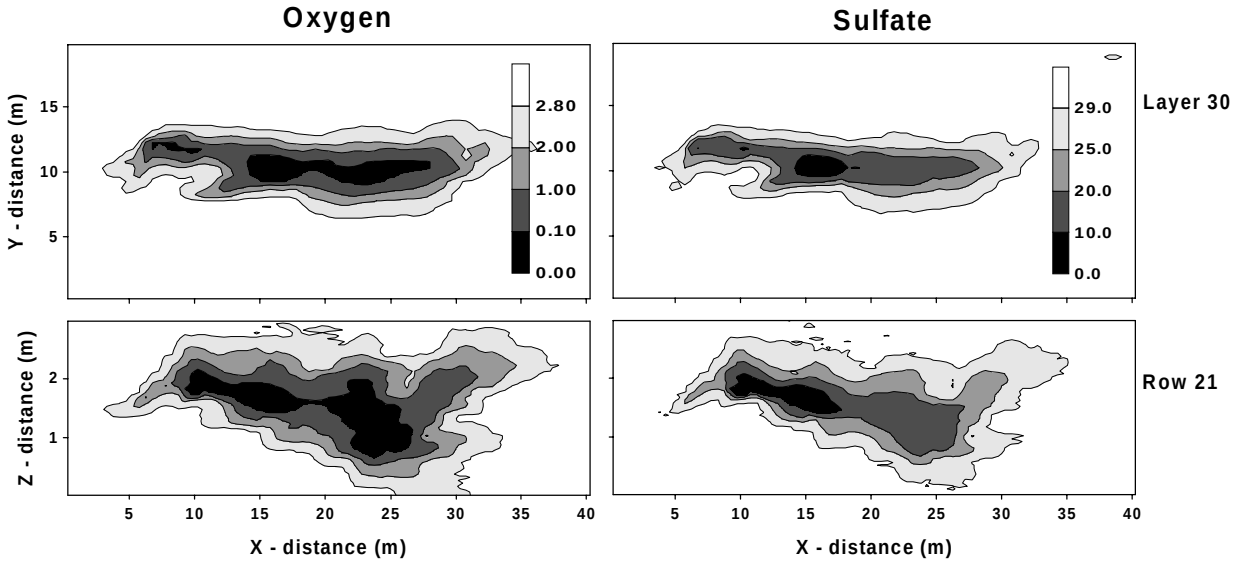

Figure 5.5. Distribution of the electron acceptors oxygen and sulfate in a horizontal slice (layer 30) and a vertical slice (row 21) through the center of the model domain at 2000 days. Each scale bar also applies to the figure below, with dimensions of g m^{-3}. Vertical (z-direction) scale is exaggerated.

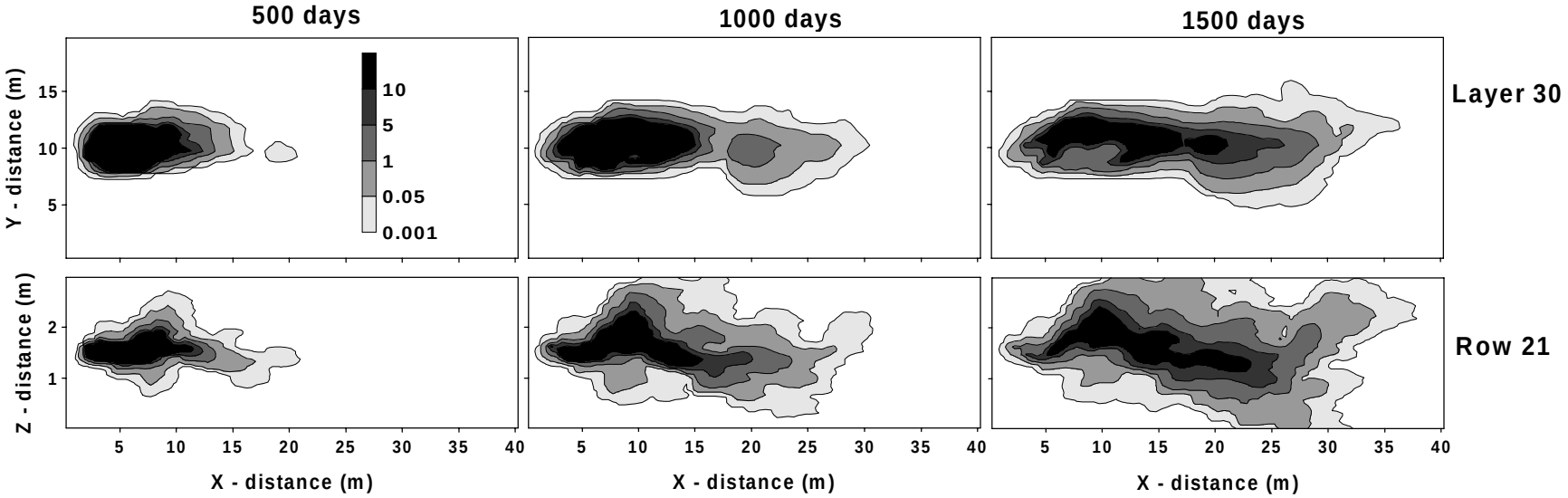

Figure 5.6. Distribution of the product H_2S in a horizontal slice (layer 30) and a vertical slice (row 21) through the center of the model domain at 500, 1000, and 1500 days. The scale bar applies to all six figures, with dimensions of g m^{-3}. Vertical (z-direction) scale is exaggerated.

5.5.2 Analysis of spatial moments

In order to assess the overall rate of biodegradation and H_2S production, the total masses of hydrocarbon, tracer, and H_2S were calculated as the zero order moments (M_{000}) in equation (5.2). In all cases, the total mass of tracer remained constant during the 2000 day simulation (data not shown), since there was no mechanism for mass loss of tracer. This conservation of tracer mass suggests minimal numerical error in the simulations. When sulfate was not simulated (making oxygen the sole EA), the EA concentration was relatively small compared to the hydrocarbon concentration. From 0 to 10 days, the hydrocarbon mass decreases by approximately 2 g as the available oxygen in the injection zone reacts quickly with the slug of hydrocarbon (Figure 5.7). This occurs because the aerobic biomass of 0.1 g m^{-3} roughly corresponded to 3.33 x 10^5 cells cm^{-3}, assuming a cell volume of 1 μm^3 and cell density of 1.0 g cm^{-3}. This number of cells and the high $\nu^{max}_{x,ls,le}$ for oxygen allow significant aerobic utilization of hydrocarbon substrates to occur without an observable lag period. After 10 days, the rate of loss of hydrocarbon mass is small (Figure 5.7) because oxygen must be transported into the relatively small zone of contamination. The rate increases with time as hydrocarbon disperses over a larger area of the domain and has access to more oxygen. Overall, the loss curve is concave down, which is the opposite of a first order decay model, where the rate of mass loss is directly proportional to the hydrocarbon concentration, and the loss curve is concave up.

For the base case, the total mass of hydrocarbon coincides with the "oxygen only" curve during the first 100 days (Figure 5.7), suggesting a lag in the utilization of sulfate. This occurs because the biomass of sulfate reducers is initially low, and the rate of sulfate reduction is much lower than aerobic degradation. As a result, the sulfate reducing microbes have to grow over a period of approximately 100 days before the population begins to exert a significant impact on biodegradation. From 100 to 250 days, the hydrocarbon mass shows a rapid decrease, which may be attributed to the activation of sulfate reduction following the utilization of oxygen. From 350 to 1000 days, the rate of mass loss is constant (i.e. zero order) over time, suggesting the hydrocarbon concentration, which is decreasing, is not the limiting factor in biodegradation.

After 1000 days, the mass loss curve is concave up, suggesting that the rate of mass loss is first order with respect to the decreasing hydrocarbon concentration.

In Case 2, the variability in the hydraulic conductivity field (as parameterized by $\sigma_{\ln K_h}$) has little effect on hydrocarbon mass loss or H_2S production at early times (Figure 5.8). However, after 500 days in Case 2a, the low value of $\sigma_{\ln K_h}$ leads to less spreading of hydrocarbon and EA, and less hydrocarbon mass is biodegraded (Figure 5.8A). Conversely, a high value of $\sigma_{\ln K_h}$ leads to slightly increased biodegradation due to additional spreading and greater mixing of hydrocarbon and EA. In Case 3, both the low correlation scale (η) and the high η lead to greater biodegradation (Figure 5.9), although the effect is minimal by the end of the simulation at 2000 days. For low η, the values of K_h are essentially random, and the lack of correlation between adjacent nodes allows greater mixing of hydrocarbon and EA relative to the base case. For high η, it is possible that the greater correlation creates more connected channels of high K_h zones. Thus, the hydrocarbon is transported more quickly out of the low K_h injection zone, and gains access to a greater mass of EA than in the base case. When the parameters K_h, $\nu_{x,ls,le}^{max}$, and M_x are allowed to be stochastic Case 4, (Figure 5.10) there is little effect on the rate of mass loss, whether or not the parameters are correlated or not. This suggests that variability in the biodegradation rate parameters is less significant than variability in the porous medium.

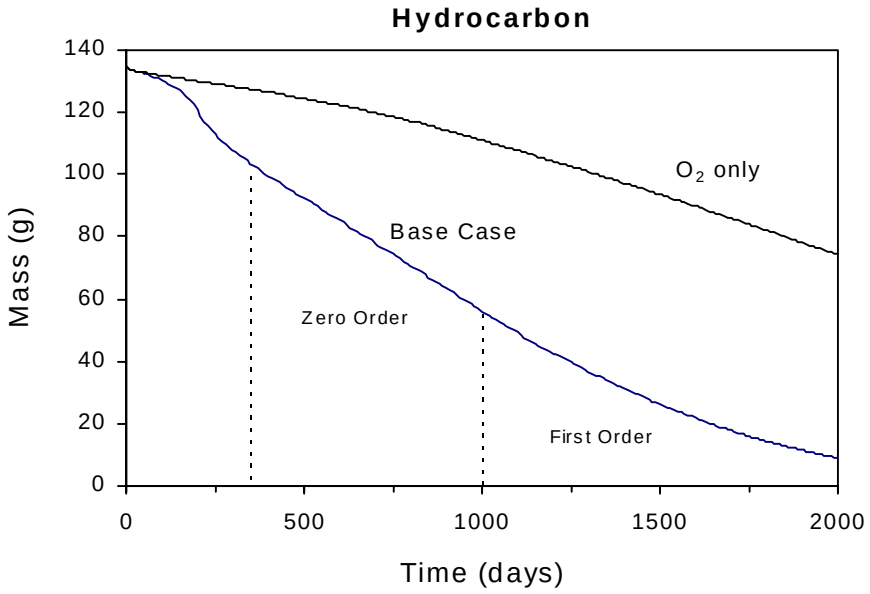

Figure 5.7. Total mass of hydrocarbon remaining in the model domain versus time for the base case and the case where oxygen (O_2) only was simulated.

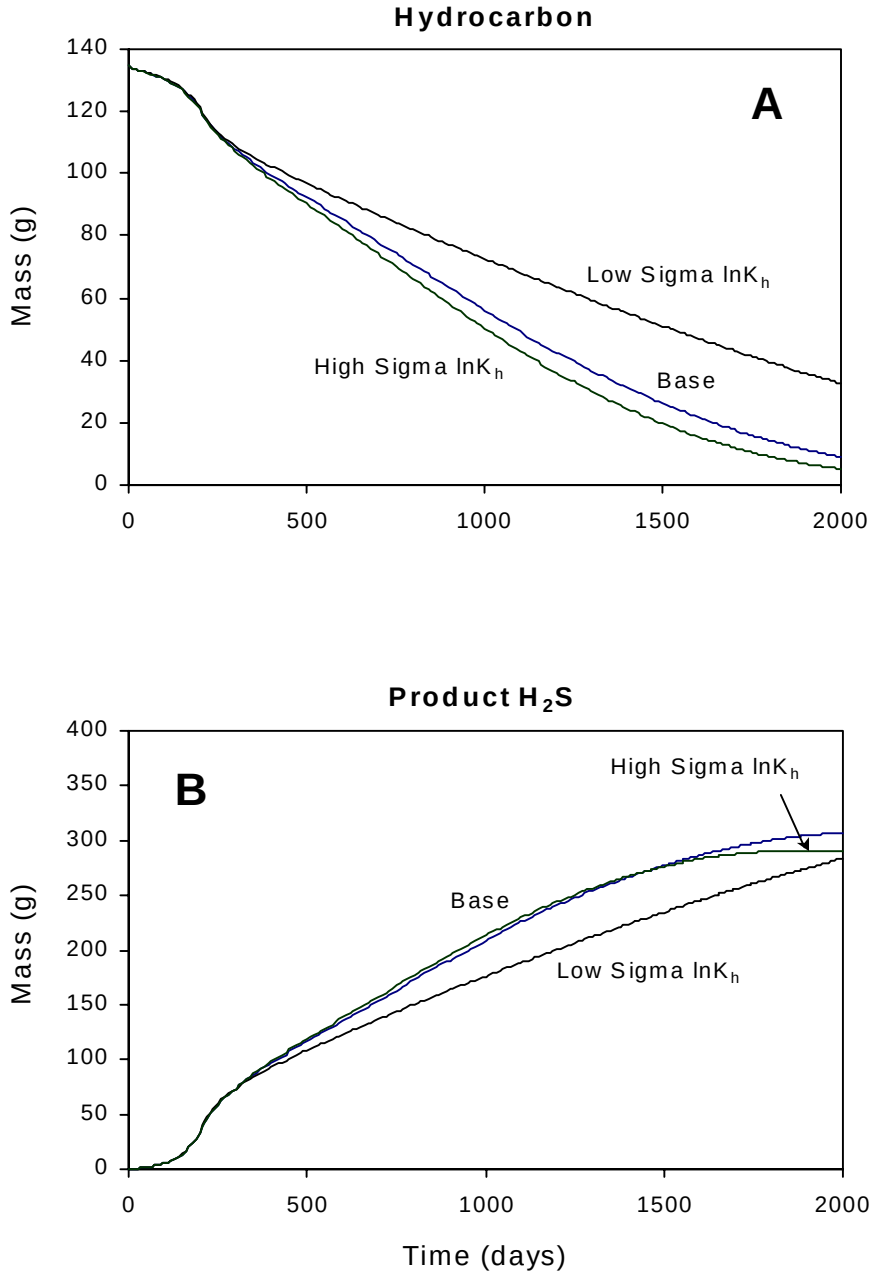

Figure 5.8. Total mass of hydrocarbon (A) and total mass of H_2S (B) remaining in the model domain versus time for the base case ($\sigma_{\ln K_h}$ = 1.0) versus case 2a with low sigma $\ln K_h$ ($\sigma_{\ln K_h}$ = 0.5) and Case 2b with high sigma $\ln K_h$ ($\sigma_{\ln K_h}$ = 1.25).

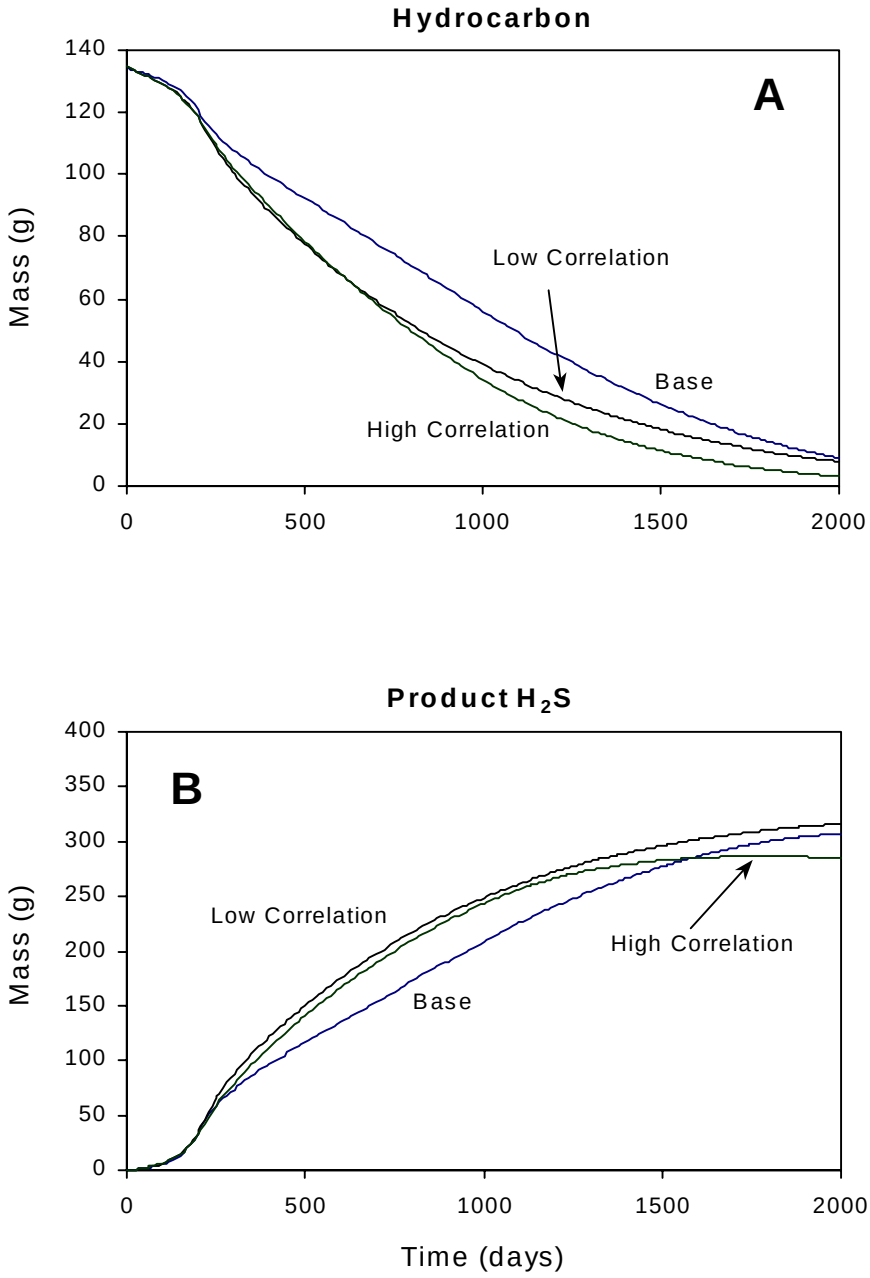

Figure 5.9. Total mass of hydrocarbon (A) and total mass of H_2S (B) remaining in the model domain versus time for the base case (η = 1.5 m) versus Case 3a with low correlation scale (η = 0.5 m) and Case 3b with high correlation scale (η = 3.0 m).

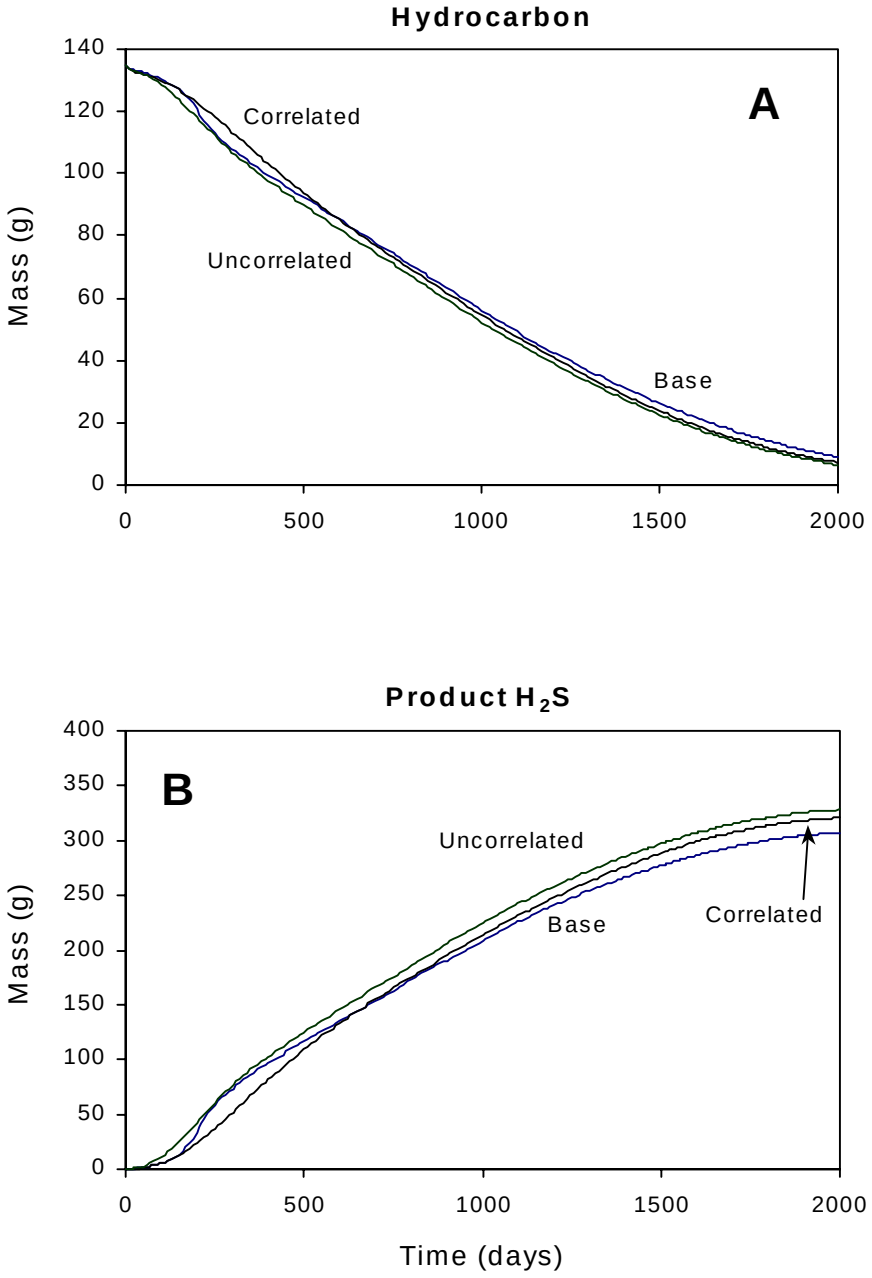

Figure 5.10. Total mass of hydrocarbon (A) and total mass of H_2S (B) remaining in the model domain versus time for the base case versus Case 4a with stochastic, correlated K_h, $\nu^{max}_{x,ls,le}$ and M_x and Case 4b with stochastic, uncorrelated K_h, $\nu^{max}_{x,ls,le}$ and M_x.

In order to depict average plume behavior for the base case, the time evolution of the centers of mass, velocities, and spatial standard deviations were computed from the spatial moments (equations 5.2 to 5.6) of the tracer and hydrocarbon. At initial time, Figure 5.11 shows that the center of mass is located at the center of the injection zone (x_c = 4.0 m, y_c = 10.0 m, and z_c = 1.50 m). The location of x_c increases over time as the hydrocarbon and tracer plumes travel down-gradient (Figure 5.11A). As time progresses, x_c for the tracer becomes greater than the hydrocarbon, but the hydrocarbon center of mass travels further in the z-direction (Figure 5.11C). In all cases, the maximum value of x_c occurs at 2000 days, and this maximum value is shown in Figure 5.12 for the base case, the "oxygen only" case, and Cases 2 through 4. In most cases, the tracer moves significantly farther than the hydrocarbon; however, for Cases 2a and 3a, low $\sigma_{\ln K_h}$ and correlation scale (η) lead to little difference in tracer versus hydrocarbon movement. As compared to the base case, the high $\sigma_{\ln K_h}$ in Case 2b causes the maximum x_c to increase for the tracer and decrease for the hydrocarbon. Thus, increased soil variability can increase the mobility of a tracer plume, while decreasing the mobility of a biodegradable plume. This may be explained by the high $\sigma_{\ln K_h}$ allowing greater access to EAs, which increases biodegradation and reduces plume mobility.

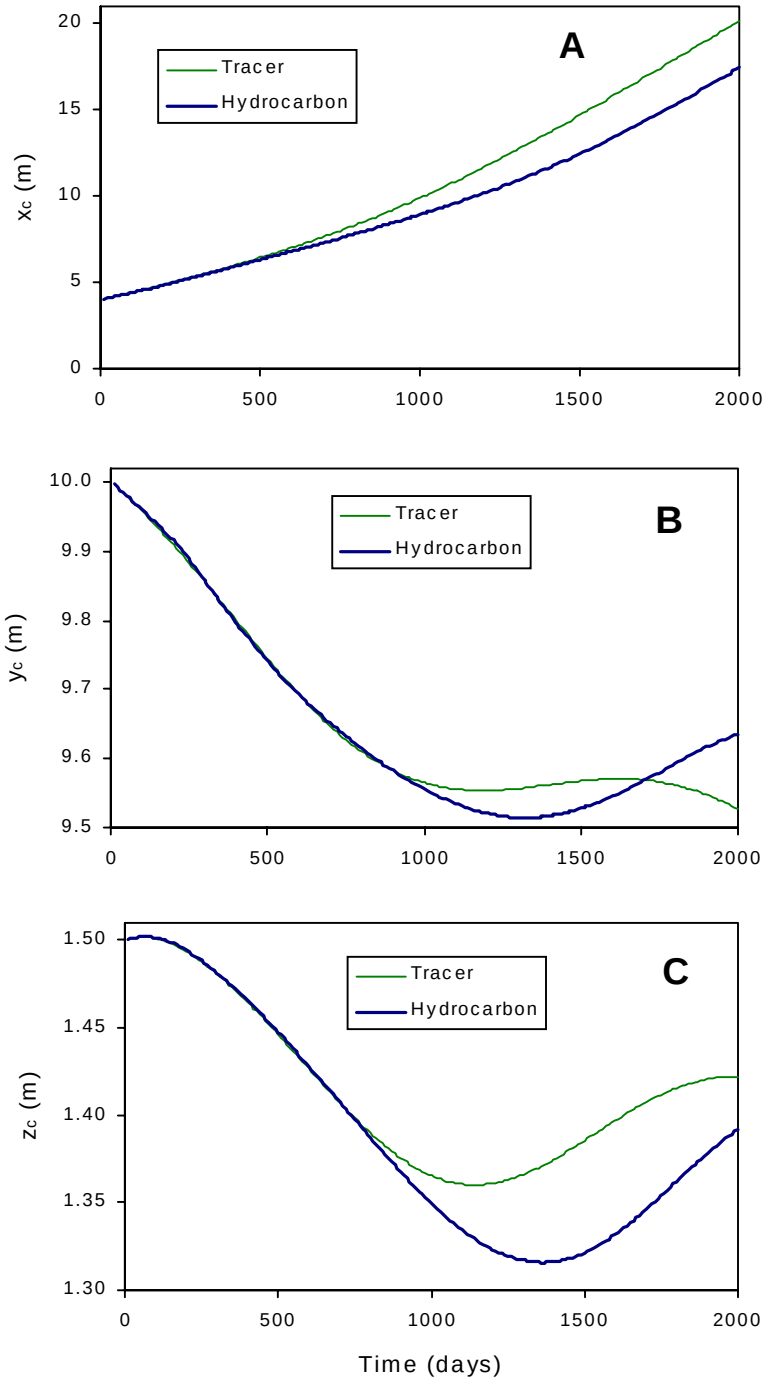

Figure 5.11. Location of the center of mass in the x-direction (A), the y-direction (B), and the z-direction (B) of the solute plumes versus time for the base case.

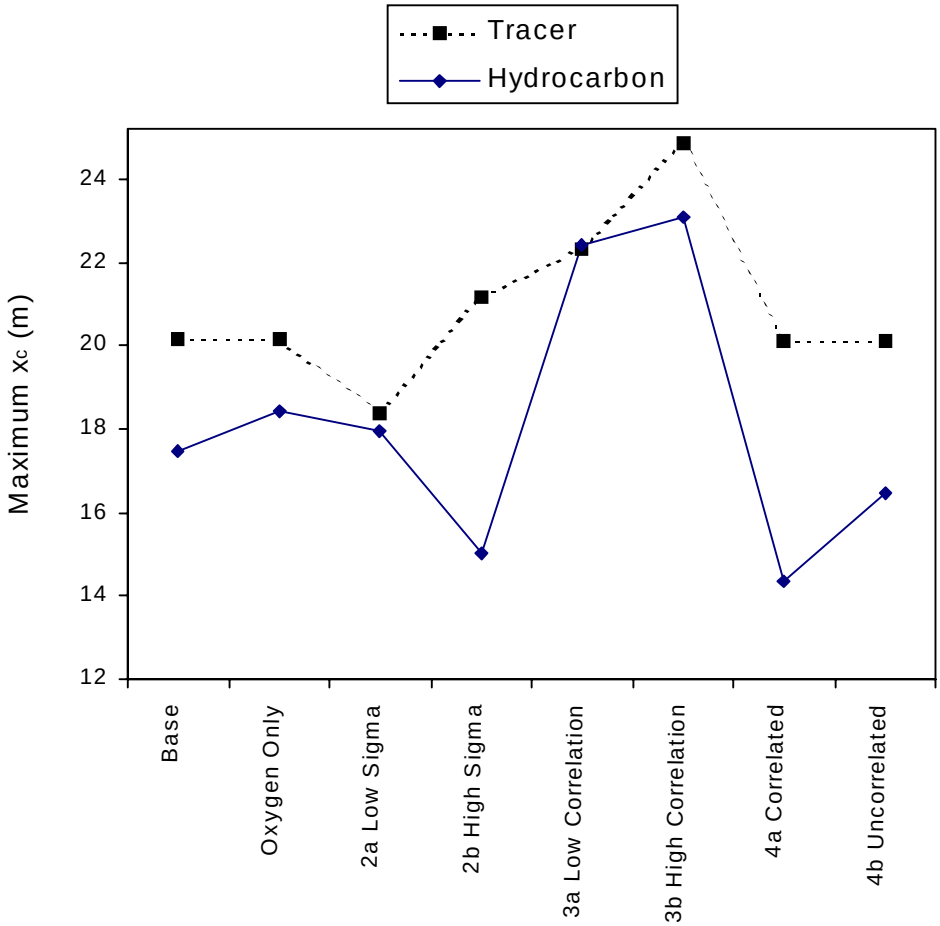

Figure 5.12. Maximum values of the location of the center of mass (x_c) for the hydrocarbon and tracer in the base case, the "oxygen only" case, and Cases 2 through 4.

For the given model domain and boundary conditions, a homogeneous hydraulic conductivity field would produce a constant x-velocity of 0.0071 m day^{-1}, and the y and z-velocities would be zero. In the heterogeneous soil, it is expected that v_x, v_y, and v_z (as computed from equation 5.5) will be variable, but they should not deviate greatly from the homogeneous values, especially as the plumes spread over a sufficiently large number of correlation scales, and irregular movements are averaged out. In the base case, the solute injection occurs in a zone of low permeability (see layer 30 in Figure 5.3), so v_x is initially lower than 0.0071 m day^{-1} (Figure 5.13A). Over time, the plumes find their way into the more permeable regions of the domain, and the velocity increases above the expected average. The tracer reaches its maximum velocity of 0.011 m day^{-1} at approximately 1700 days, after which time v_x begins to diminish. In contrast, v_x for the hydrocarbon is still increasing at 2000 days, perhaps because it has not spread over as many correlation scales as the tracer, and a greater percentage of the plume is in the high permeability zone.

In the y and z-directions, the velocities of the tracer and the hydrocarbon tend to oscillate about the respective axis origins (Figure 5.13B and C), and the departures from zero become smaller with time, especially for the tracer. At later times, the hydrocarbon shows larger oscillations than the tracer in both the y and z-directions, again suggesting that the smaller hydrocarbon plume has a lesser tendency to follow average behavior. In addition, at early times, v_y for the hydrocarbon shows erratic changes over time that are not seen in the tracer. Overall, the effect of biodegradation tends to make the velocity of the hydrocarbon plume more erratic than the tracer.

The minimum and maximum values of v_x are shown in Figure 5.14 for the base case, the "oxygen only" case, and Cases 2 through 4. In most cases, the tracer moves faster than the hydrocarbon, although this trend is reversed for Case 3a with the low correlation scale (η). Cases 3a also shows the smallest difference in the maximum and minimum velocities. This occurs because the low η makes K_h essentially random, and no large zones of high or low K_h exist in the domain. Thus, the overall velocity does not tend to deviate greatly from the average rate. Both the maximum and minimum velocities are greater than the 0.0071 m day^{-1} expected in a homogeneous soil. This suggests that the solutes tend to flow preferentially through connected paths of high conductivity. In Case 4a, the maximum v_x for the hydrocarbon is much

less than the tracer. This occurs because of the correlation in the stochastic parameters, such that the zones of high K_h also have high $\nu^{max}_{x,ls,le}$, and M_x. Thus the rate of biodegradation is fastest in the high conductivity zones, and the degradation of mass in these areas tends to slow the overall plume velocity.

Plume spreading, as indicated by the spatial standard deviations σ_{ii} (Figure 5.15), is consistently greater for the tracer than the hydrocarbon in all directions. This is expected since biodegradation occurs at the edges of the hydrocarbon plume and limits its outward expansion. In the y-direction, the hydrocarbon plume actually contracts over time, as shown by the decreasing value of σ_{yy} (Figure 5.15B). For the base case, the "oxygen only" case, and Cases 2 through 4, the maximum values of σ_{ii} are shown in Figure 5.16. As expected, the low value of $\sigma_{\ln K_h}$ in Case 2a leads to less spreading than in Case 2b with high $\sigma_{\ln K_h}$. The same trend occurs to a lesser degree with the correlation scale, probably because a high correlation scale leads to more connected channels of high permeability, and these channels allow greater plume spreading.

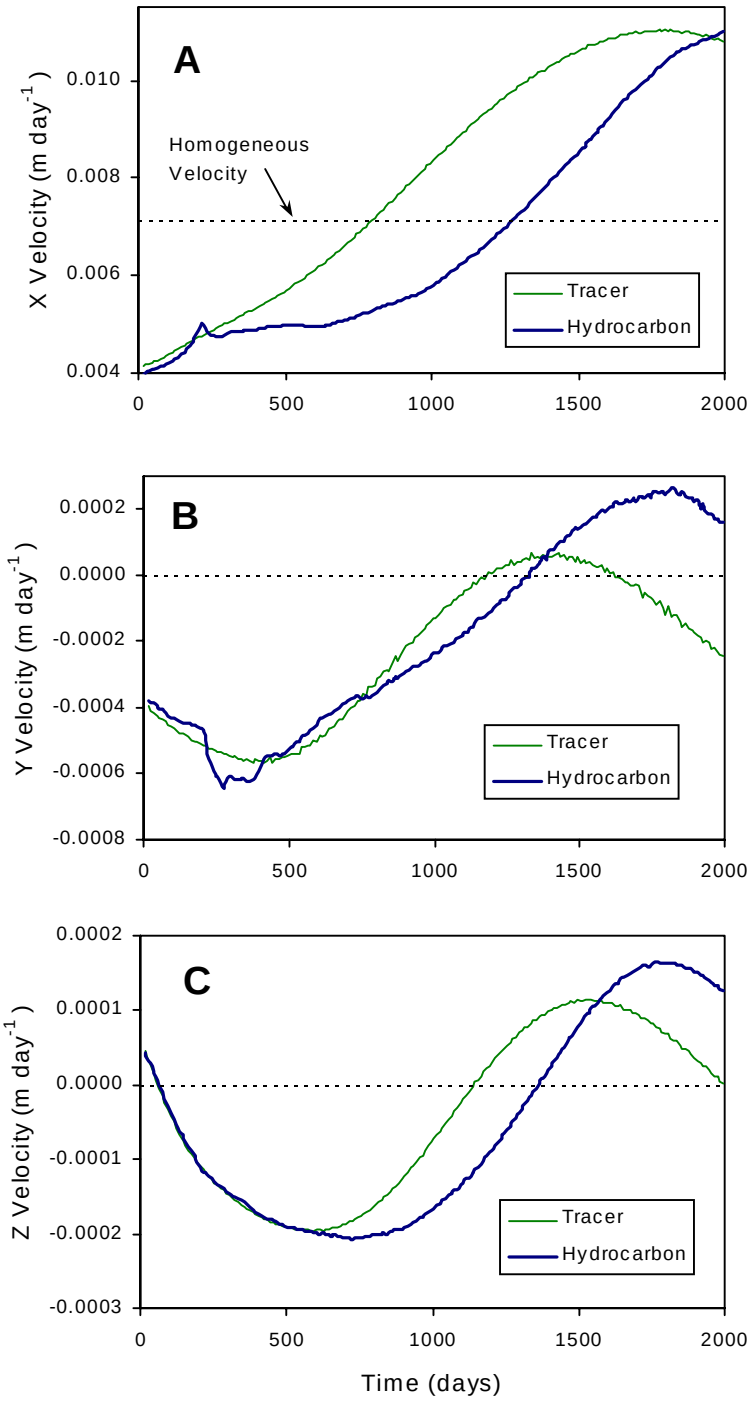

Figure 5.13. Velocity of the center of mass in the x-direction (A), the y-direction (B), and the z-direction (C) of the solute plumes versus time for the base case. The average x-velocity as calculated for a homogeneous porous medium is also depicted.

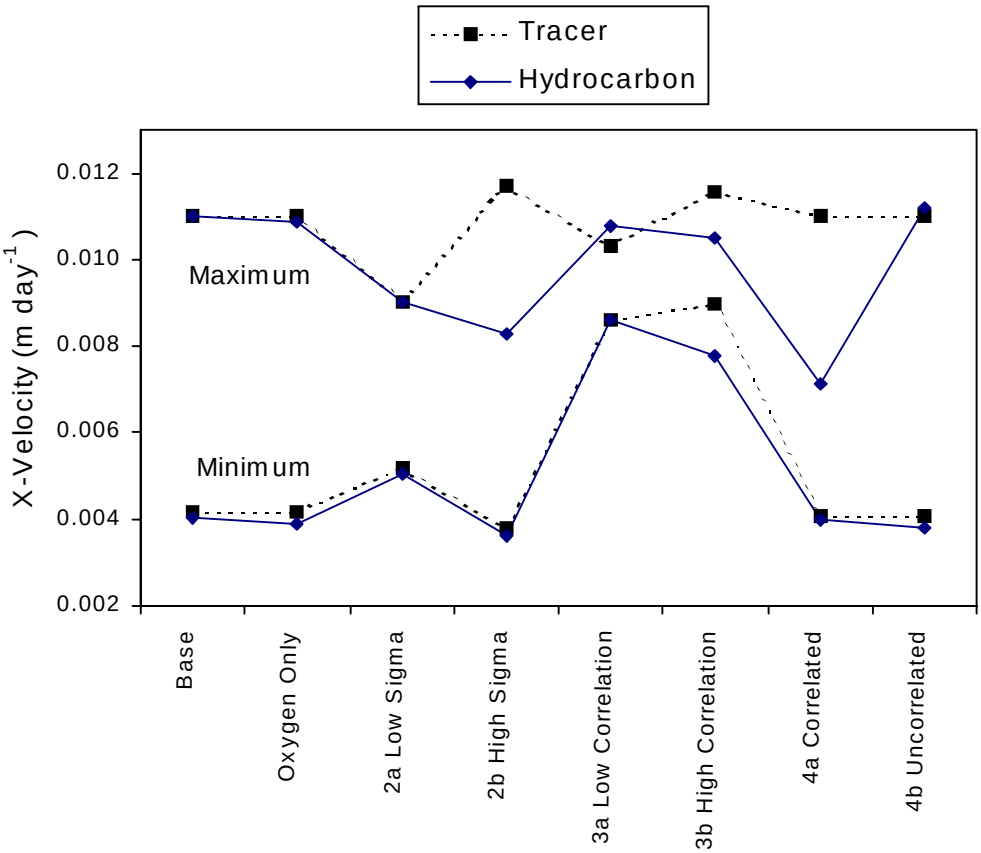

Figure 5.14. Minimum and maximum values of the x-velocity of the hydrocarbon and tracer in the base case, the "oxygen only" case, and Cases 2 through 4.

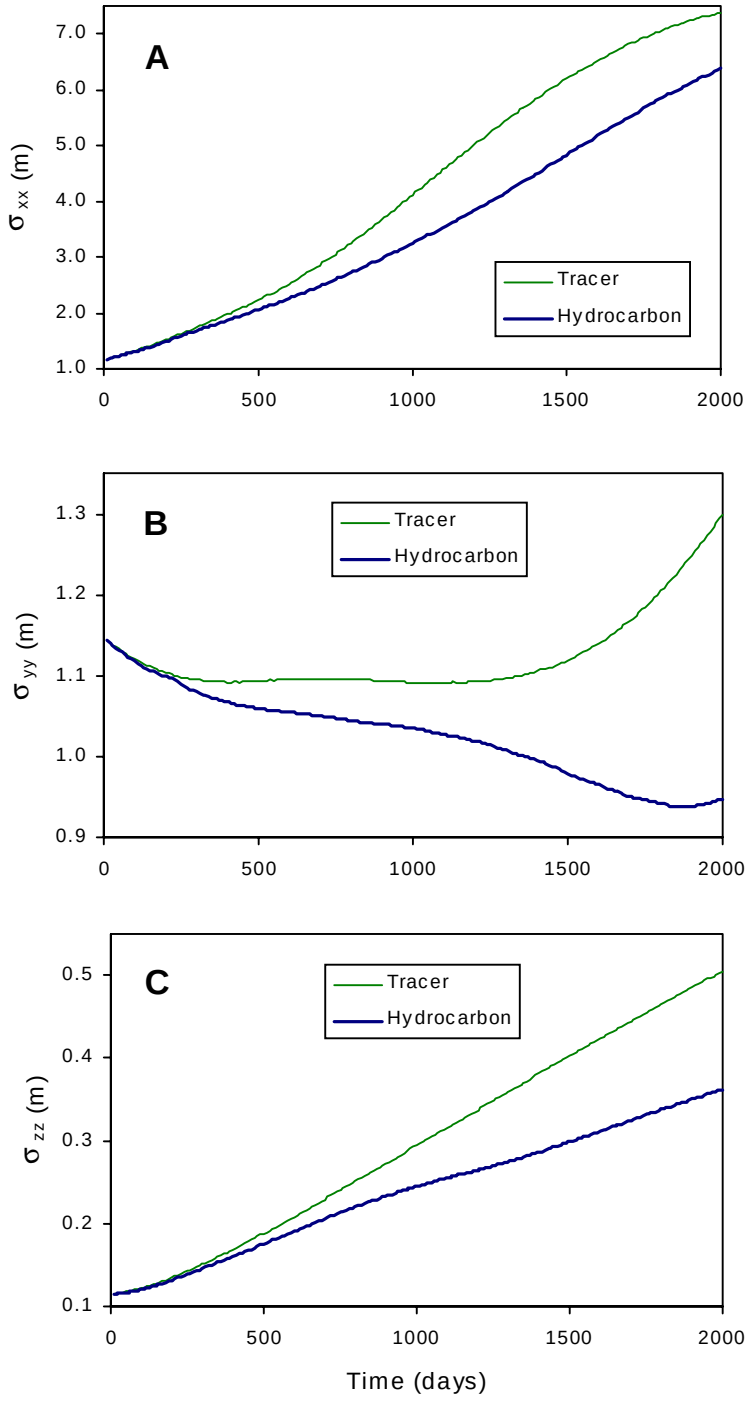

Figure 5.15. Spatial standard deviations (σ_{ii}) of the solute plumes in the x-direction (A), the y-direction (B), and the z-direction (C) versus time for the base case.

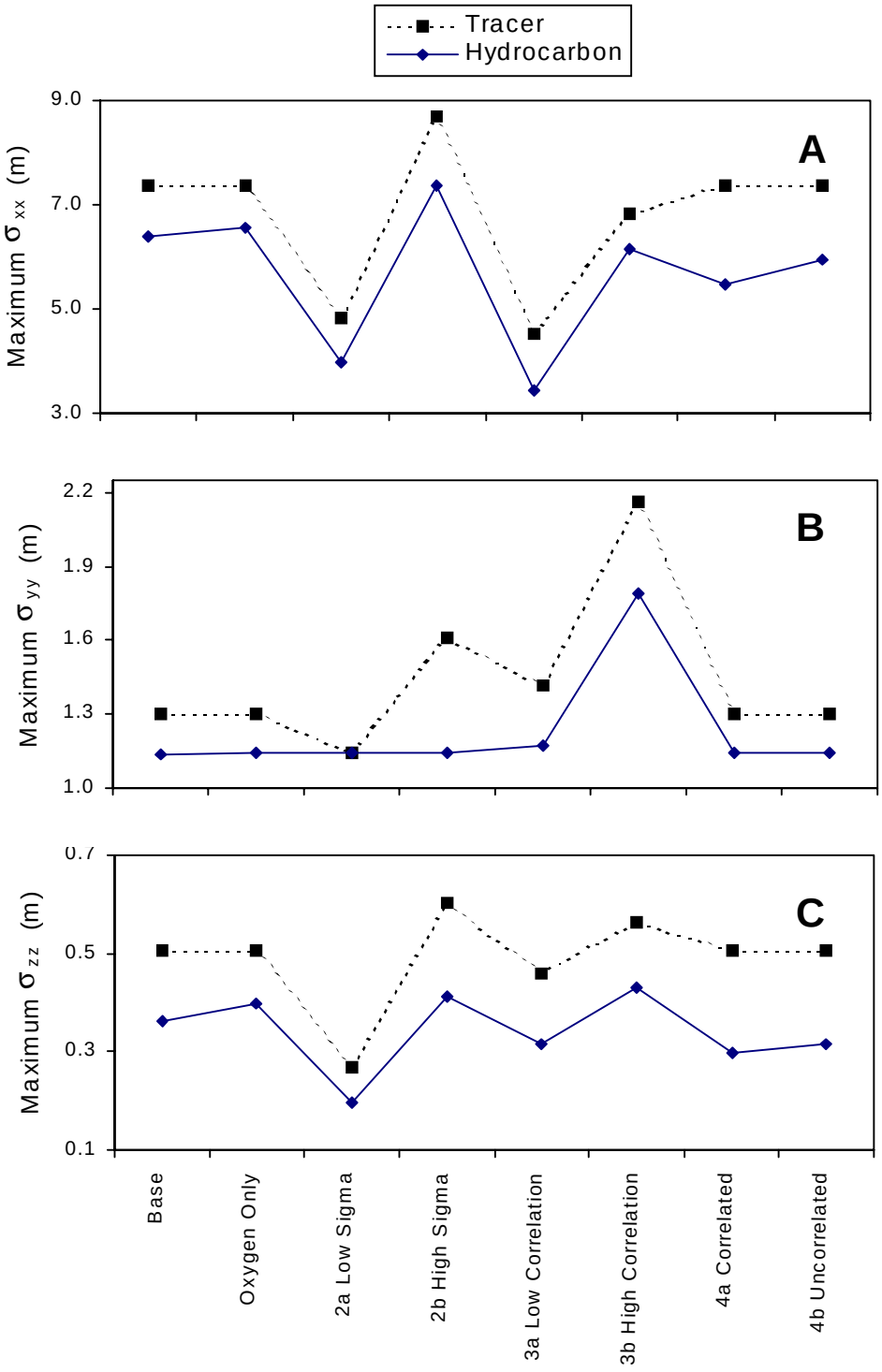

Figure 5.16. Maximum values of the spatial standard deviations (σ_{ii}) of the solute plumes in the x-direction (A), the y-direction (B), and the z-direction (C) for the base case, the "oxygen only" case, and Cases 2 through 4.

5.5.3 Statistical Analysis

The mean and the coefficients of variation (CVs) of the resident and flux hydrocarbon concentrations were computed over time by averaging over a vertical slice through the center of the model domain, transverse to the average direction of flow (i.e., column 40). For the base case, the flux averaged concentration becomes significantly greater than the resident averaged concentration at 1000 days (Figure 5.17). This suggests that the zones of high permeability are carrying a higher proportion of hydrocarbon than zones of low permeability. In addition, the flux CVs are higher than the resident CVs, indicating that variability in the plume distribution is higher when weighted by the variability of the flowrate.

For comparison, the maximum values of the mean resident and flux hydrocarbon concentrations are shown in Figure 5.18 for the base case, the "oxygen only" case, and Cases 2 through 4. The maximum value is much higher in the oxygen only case and in Case 2a with low $\sigma_{\ln K_h}$ because overall biodegradation rates are reduced when EA availability or mixing is limited. In general, the flux-averaged concentrations are greater than the average resident concentrations, although the difference is negligible in Case 3a with low correlation scale (η). This occurs because the small η makes the flow field essentially random, and the flowrates are uniformly distributed across column 40 where the average is computed.

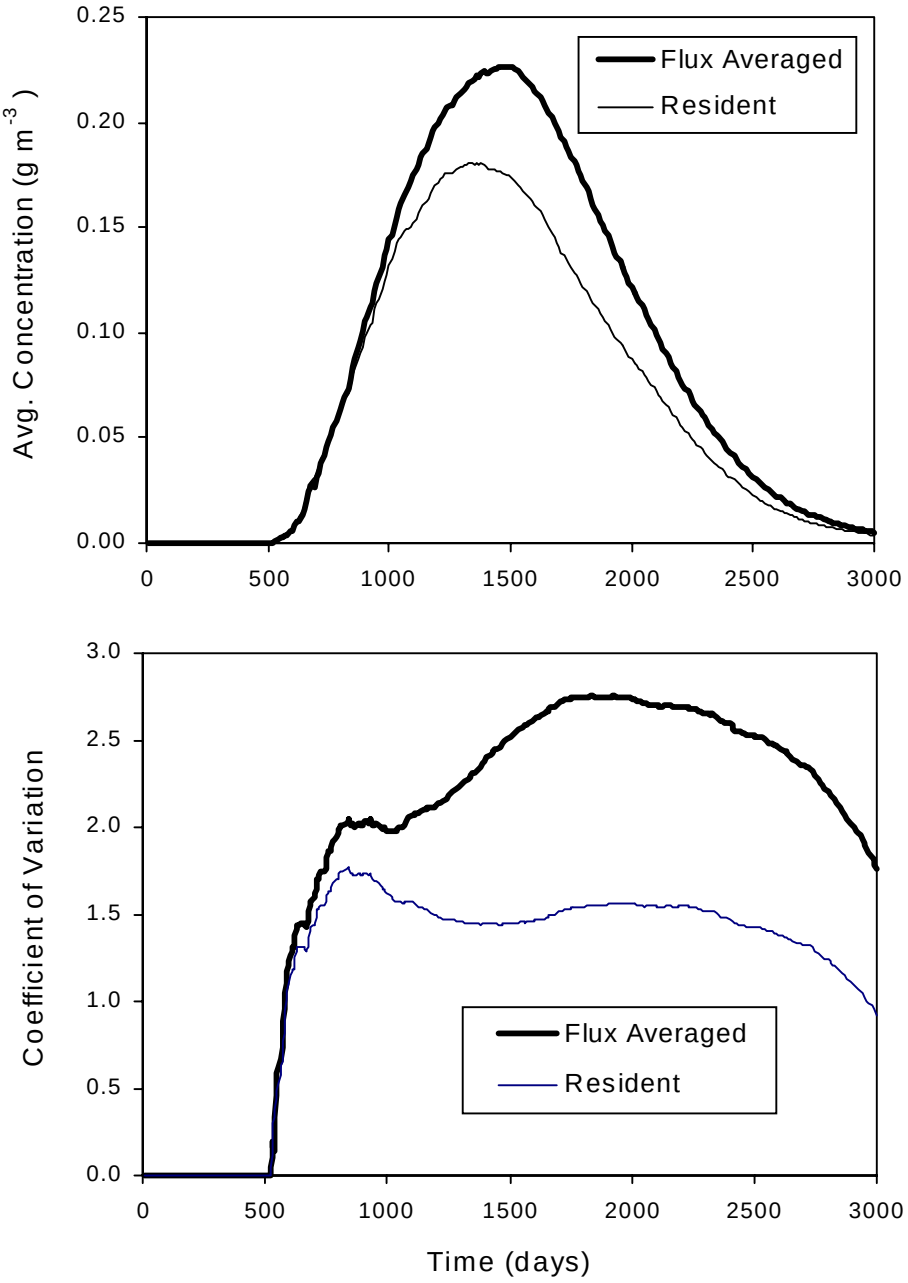

Figure 5.17. Comparison of the mean (A) and the coefficients of variation (B) of the resident and flux hydrocarbon concentrations over time. Values were obtained by averaging over a vertical slice through the center of the model domain, perpendicular to the direction of flow (i.e., column 40).

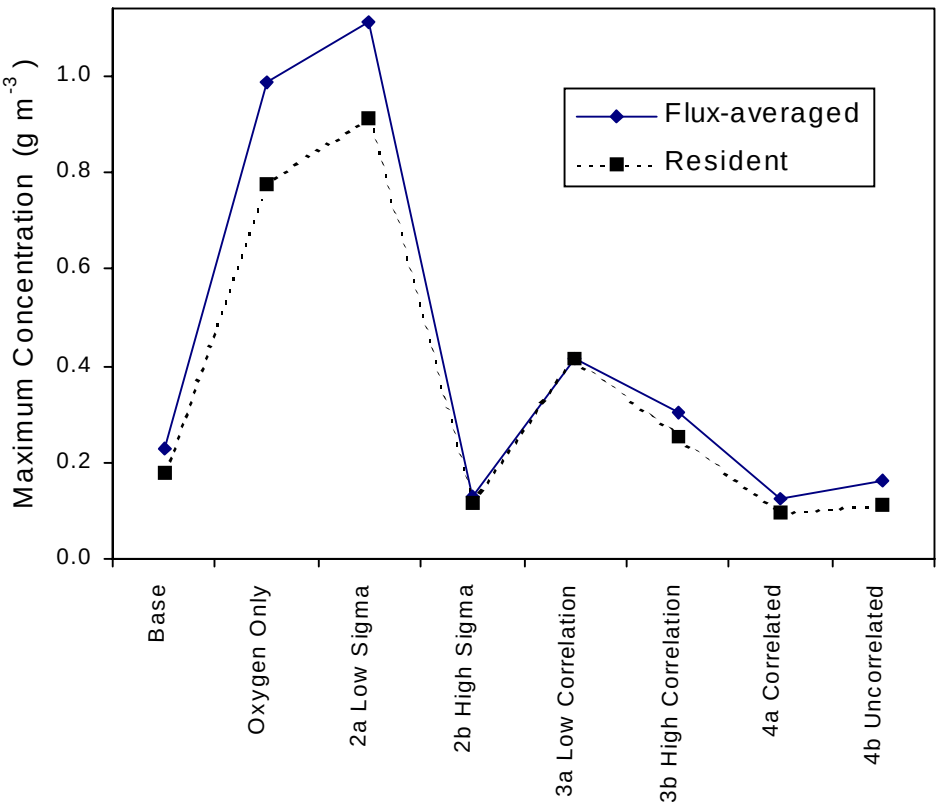

Figure 5.18. Maximum values of the resident and flux-averaged concentrations of hydrocarbon in the base case, the "oxygen only" case, and Cases 2 through 4.

5.6 Sensitivity Analysis

A sensitivity analysis was performed to measure model response to uncertainty in the input parameters. The model output examined over time was the total mass of solute for the biodegradable hydrocarbon, the nondegradable tracer, and the product H_2S. In addition, a comparison was made of the maximum values of the location of the center of mass in the x-direction (x_c), the minimum and maximum x-velocities (v_x), the maximum values of the spatial standard deviations (σ_{ii}), and the maximum values of the mean resident and flux hydrocarbon concentrations. In each case, model parameters were altered relative to the base case (Table 5.4) within reasonable ranges that have been reported in the literature (see Section 5.4.4). For Case 9b, the value of $\kappa_{le,li}$ = 9999 g m^{-3} effectively eliminates inhibition, such that sulfate reduction and aerobic respiration are allowed to occur simultaneously.

Since the initial concentrations of hydrocarbon were altered in Case 5, the total mass of hydrocarbon in Figure 5.19A is normalized by its initial mass, and the total mass of H_2S is normalized by its maximum concentration (Figure 5.19B). When the concentration of oxygen and sulfate is high relative to the hydrocarbon, the mass loss curve is concave up after 250 days, indicating that mass loss depends on the concentration of remaining hydrocarbon by a first order relationship. A simplified first order decay model might be adequate in this case, although the first order sink term would not capture the relatively slow rate of biodegradation at early times. In contrast, the mass loss curve is concave down for low EA, indicating that mass loss depends on spreading into areas having available EA. The rates of hydrocarbon mass loss and H_2S production vary significantly with these changes in initial hydrocarbon and EA concentration.

In Case 6, as the microbial biomass (M_x) decreases, the lag period that precedes rapid biodegradation and H_2S production increases (Figure 5.20). Nevertheless, the high values for M_x have little effect on the final mass of hydrocarbon at 2000 days, since hydrocarbon and EA availability ultimately limit the biodegradation rate. In contrast, low initial values for M_x have a significant effect on the final mass of hydrocarbon and H_2S at 2000 days, showing that rate limitations, and not simply hydrocarbon and EA availability, have come into effect. These same trends are observed when the maximum specific rate of substrate utilization ($\nu^{max}_{x,ls,le}$) is altered in Case 7 (Figure 5.21). In Case 8, the changes to the half saturation coefficients ($K^{e}_{x,le}$ and

$K^{s}_{x,ls,le}$) do not significantly affect the lag period; however, the high values of $K^{e}_{x,le}$ and $K^{s}_{x,ls,le}$ cause significant reductions in the utilization rate (Figure 5.22). Of all the parameters in the sensitivity analysis, the mass of hydrocarbon is least sensitive to changes in the inhibition coefficient (Figure 5.23).

Figure 5.24 shows that the maximum values of x_c are affected most significantly by high $\nu^{max}_{x,ls,le}$ (Case 7b) and low $K^{e}_{x,le}$ / $K^{s}_{x,ls,le}$ (Case 8a), while the initial concentrations of EA and hydrocarbon (Cases 5a and 5b), high M_x (Case 6b), and $\kappa_{le,li}$ (Cases 9a and 9b) have an intermediate effect. The minimum and maximum v_x, and the maximum spread in the x and z directions (σ_{xx} and σ_{zz}) are also affected most significantly by high $\nu^{max}_{x,ls,le}$ and low $K^{e}_{x,le}$ / $K^{s}_{x,ls,le}$ (Figures 5.25 and 5.26). In all cases, the flux-averaged concentration is greater than the average resident concentration (Figure 5.27) although the difference is slight in Case 5b, where the high EA concentration allows very little hydrocarbon to past through the column 40 plane.

Table 5.4. Parameter description and values for the sensitivity analysis.

	Altered Parameter Relative to Base Case	Aerobes or Oxygen	SO_4 Reducers or Sulfate	Substrate
Case 5a	Initial Conc. ($g\ m^{-3}$)	1.5	15.0	120.0
Case 5b		6.0	60.0	30.0
Case 6a	M_x ($g\ m^{-3}$)	0.01	0.001	--
Case 6b		1.0	0.1	--
Case 7a	$\nu^{max}_{x,ls,le}$ (day^{-1})	0.2	0.02	--
Case 7b		5.0	0.5	--
Case 8a	$K^e_{x,le}$ or $K^s_{x,ls,le}$ ($g\ m^{-3}$	0.1	0.1	1.0
Case 8b		2.0	2.0	20.0
Case 9a	$\kappa_{le,li}$ ($g\ m^{-3}$)	0.01	--	--
Case 9b		9999	--	--

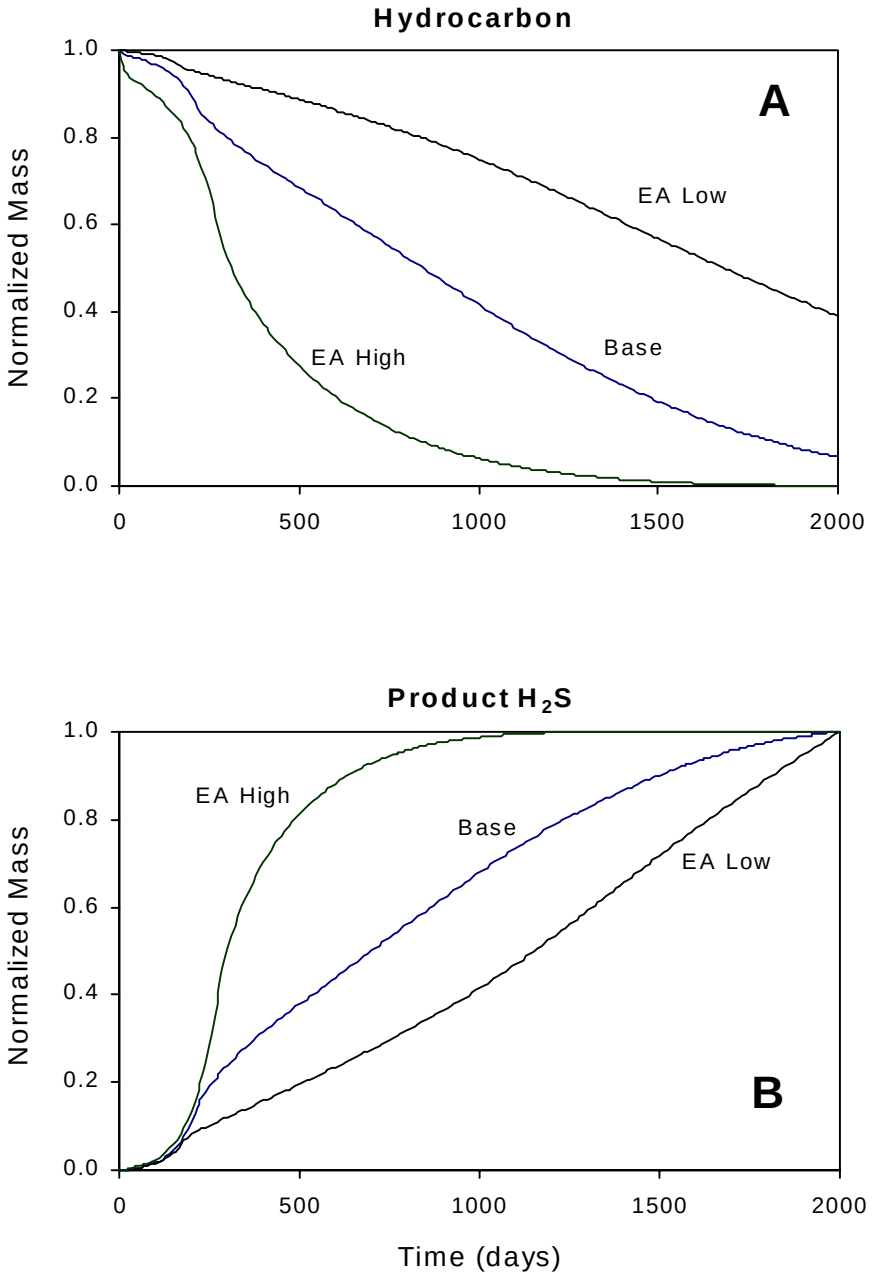

Figure 5.19. Total mass of hydrocarbon (A) and total mass of H_2S (B) remaining in the model domain versus time for the base case versus Case 5a with low EA available and Case 5b with high EA.

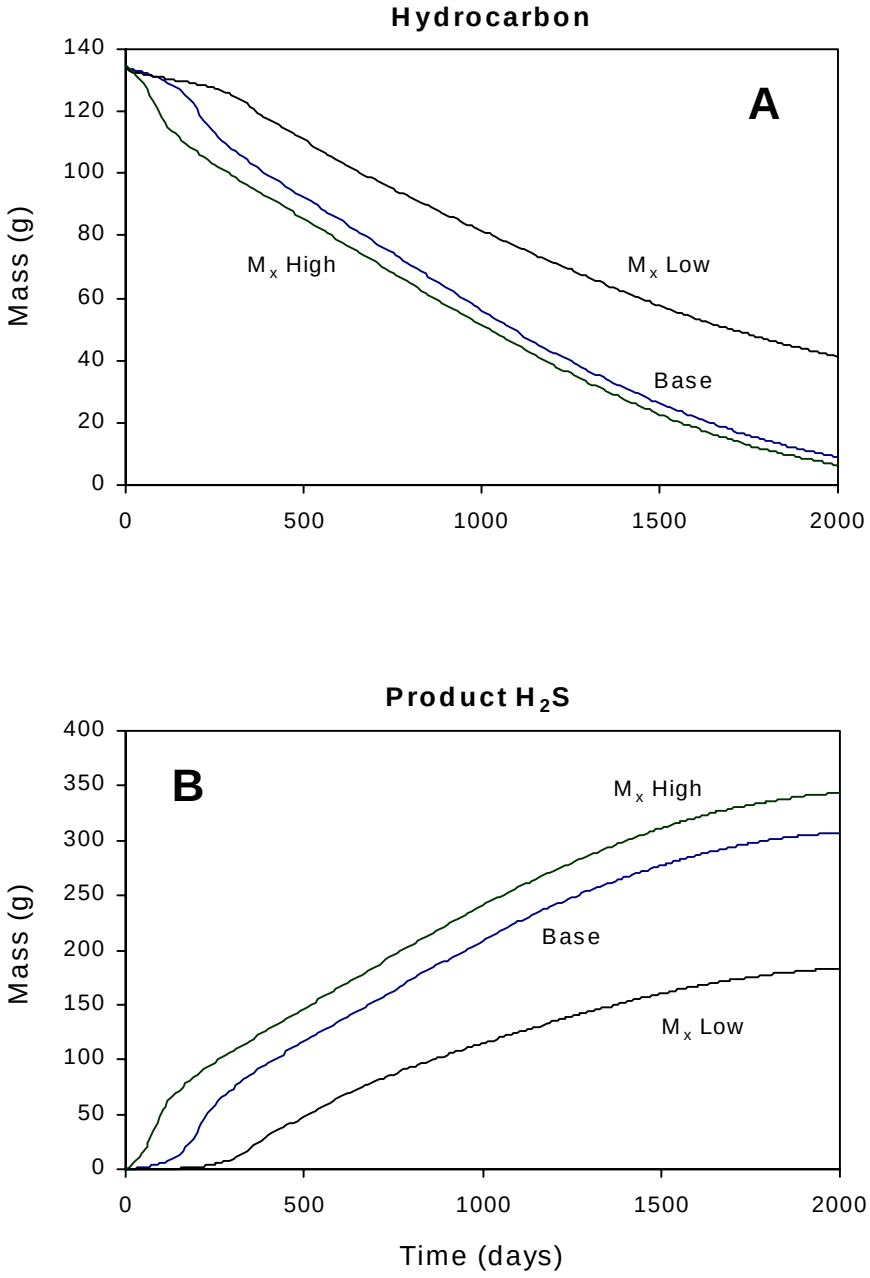

Figure 5.20. Total mass of hydrocarbon (A) and total mass of H_2S (B) remaining in the model domain versus time for the base case versus Case 6a with low initial microbial populations (M_x) and Case 6b with high initial M_x.

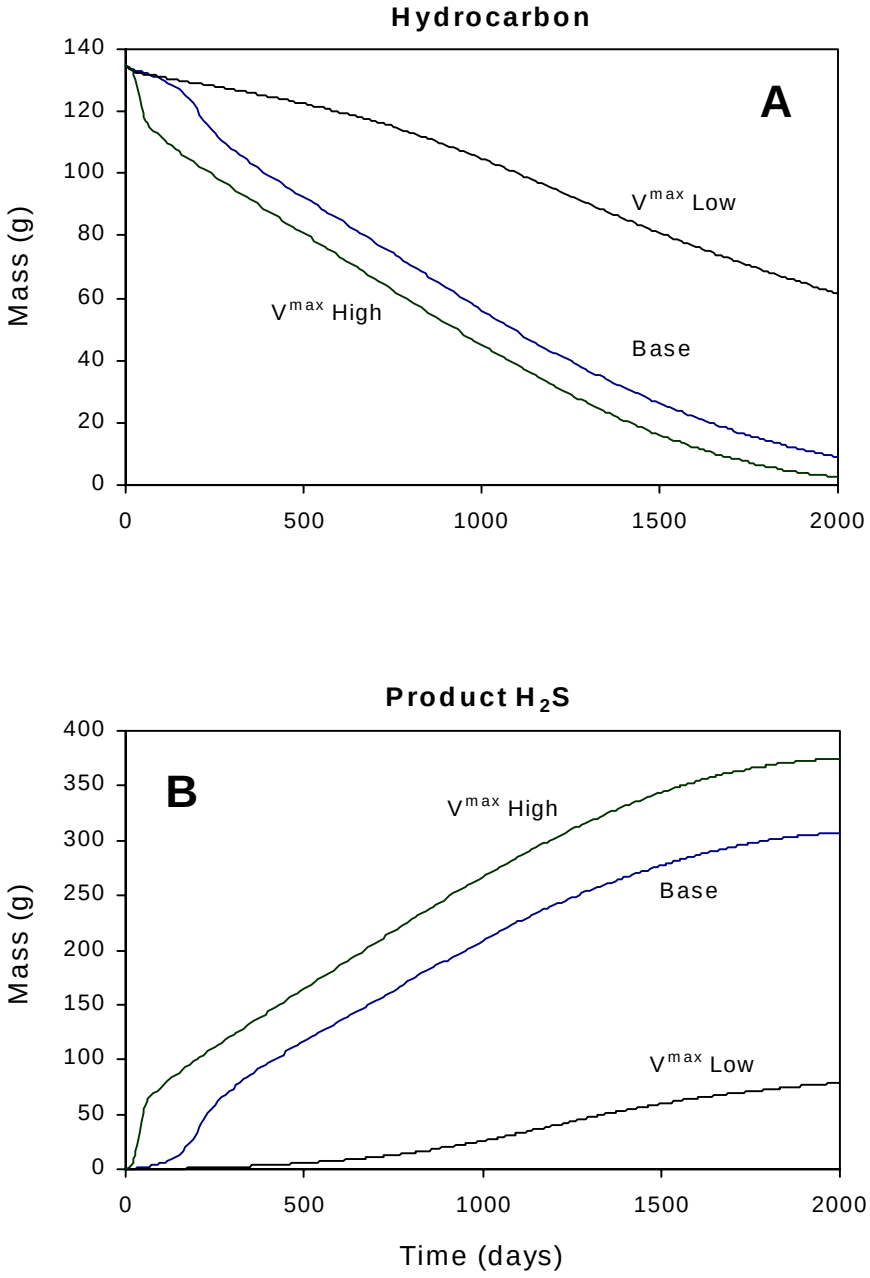

Figure 5.21. Total mass of hydrocarbon (A) and total mass of H_2S (B) remaining in the model domain versus time for the base case versus Case 7a with low maximum specific rate of substrate utilization ($\nu^{max}_{x,ls,le}$) and Case 7b with high $\nu^{max}_{x,ls,le}$.

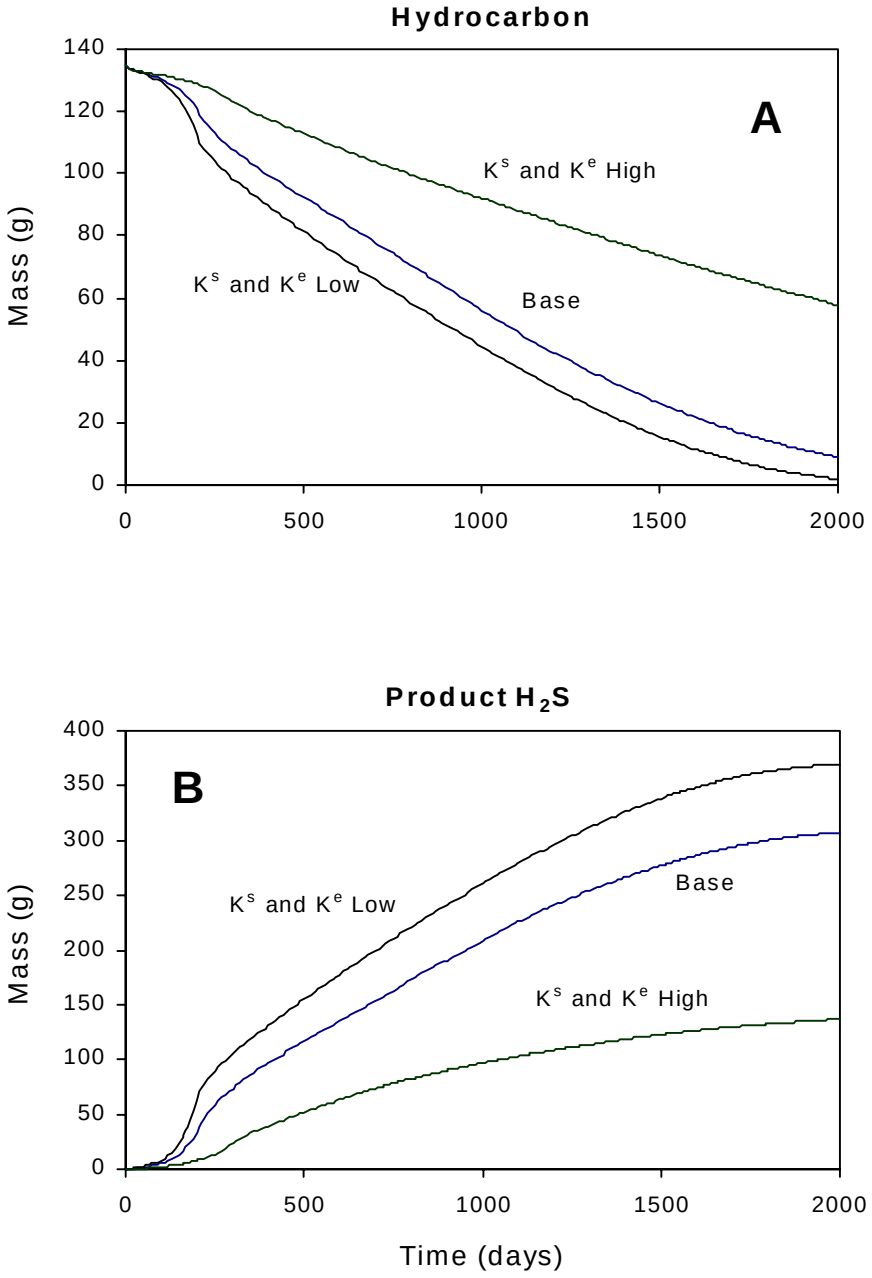

Figure 5.22. Total mass of hydrocarbon (A) and total mass of H_2S (B) remaining in the model domain versus time for the base case versus Case 8a with low half saturation constants ($K^e_{x,le}$ and $K^s_{x,ls,le}$) and Case 8b with high $K^e_{x,le}$ and $K^s_{x,ls,le}$.

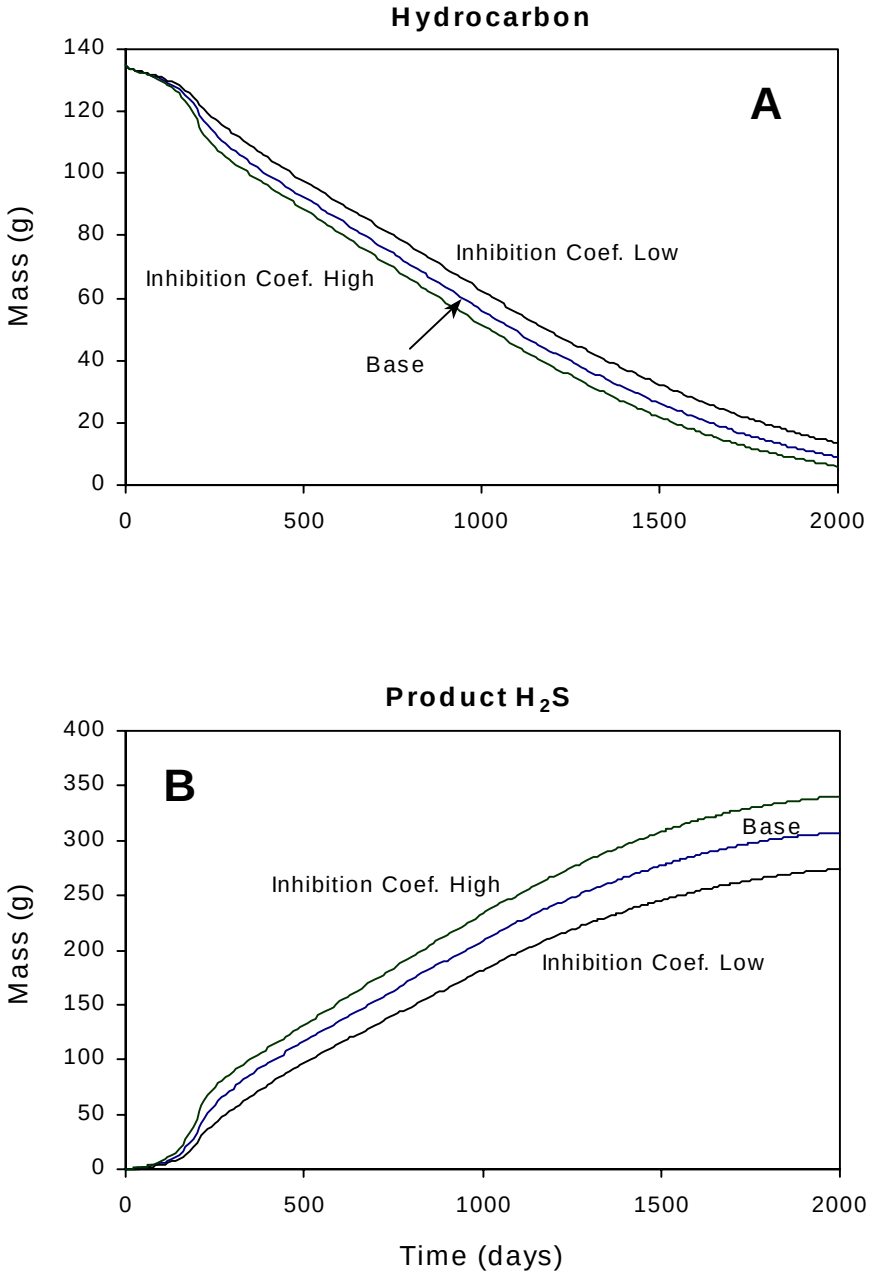

Figure 5.23. Total mass of hydrocarbon (A) and total mass of H_2S (B) remaining in the model domain versus time for the base case versus Case 9a with low inhibition coefficient ($\kappa_{le,li}$) and Case 9b with $\kappa_{le,li}$ high enough to eliminate inhibition.

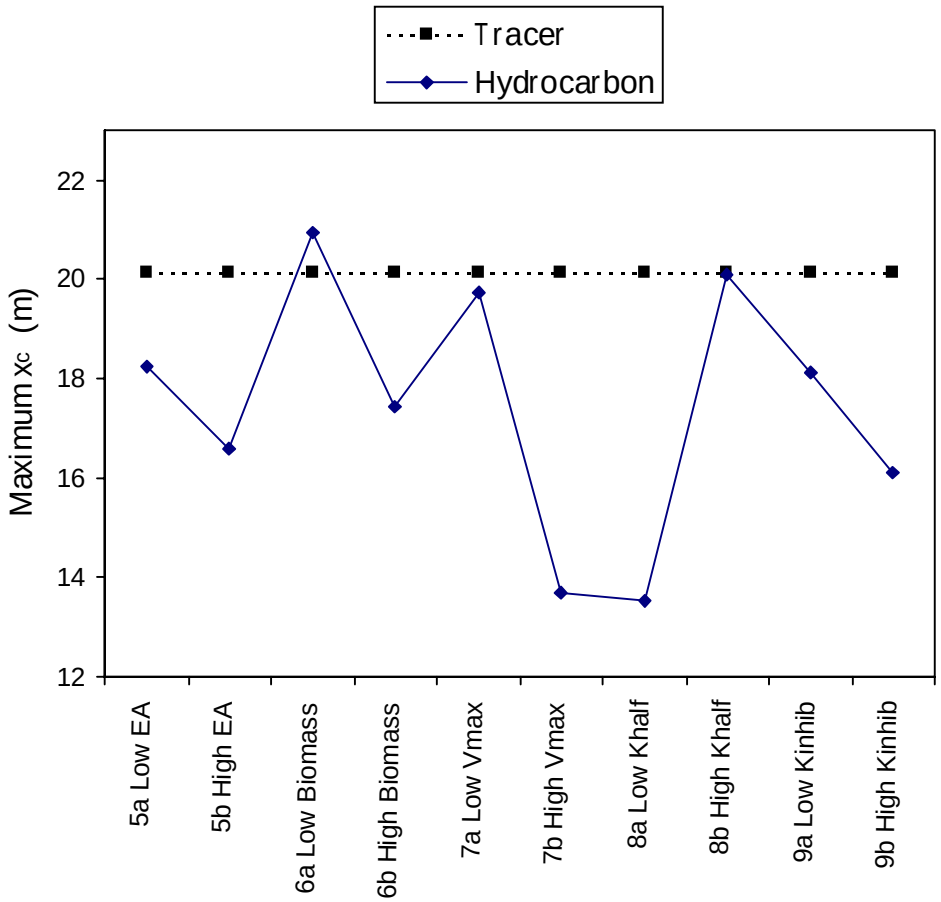

Figure 5.24. Maximum values of the location of the center of mass (x_c) for the hydrocarbon and tracer in Cases 5 through 9.

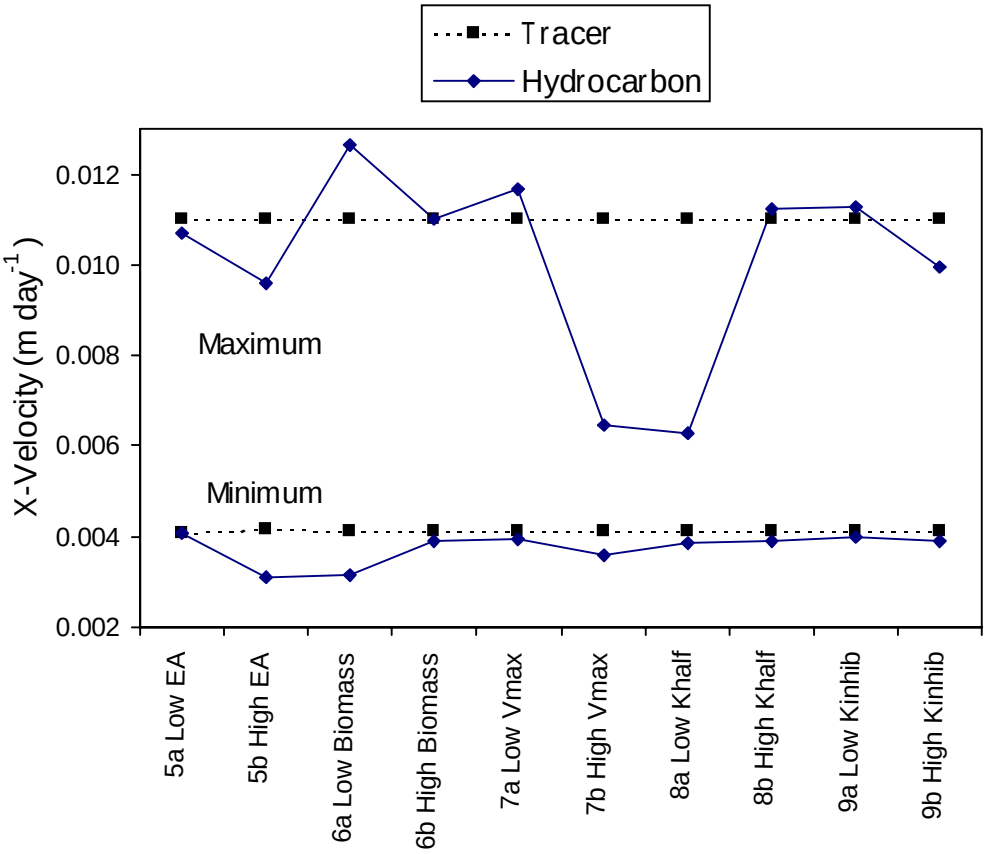

Figure 5.25. Minimum and maximum values of the x-velocity of the hydrocarbon and tracer in Cases 5 through 9.

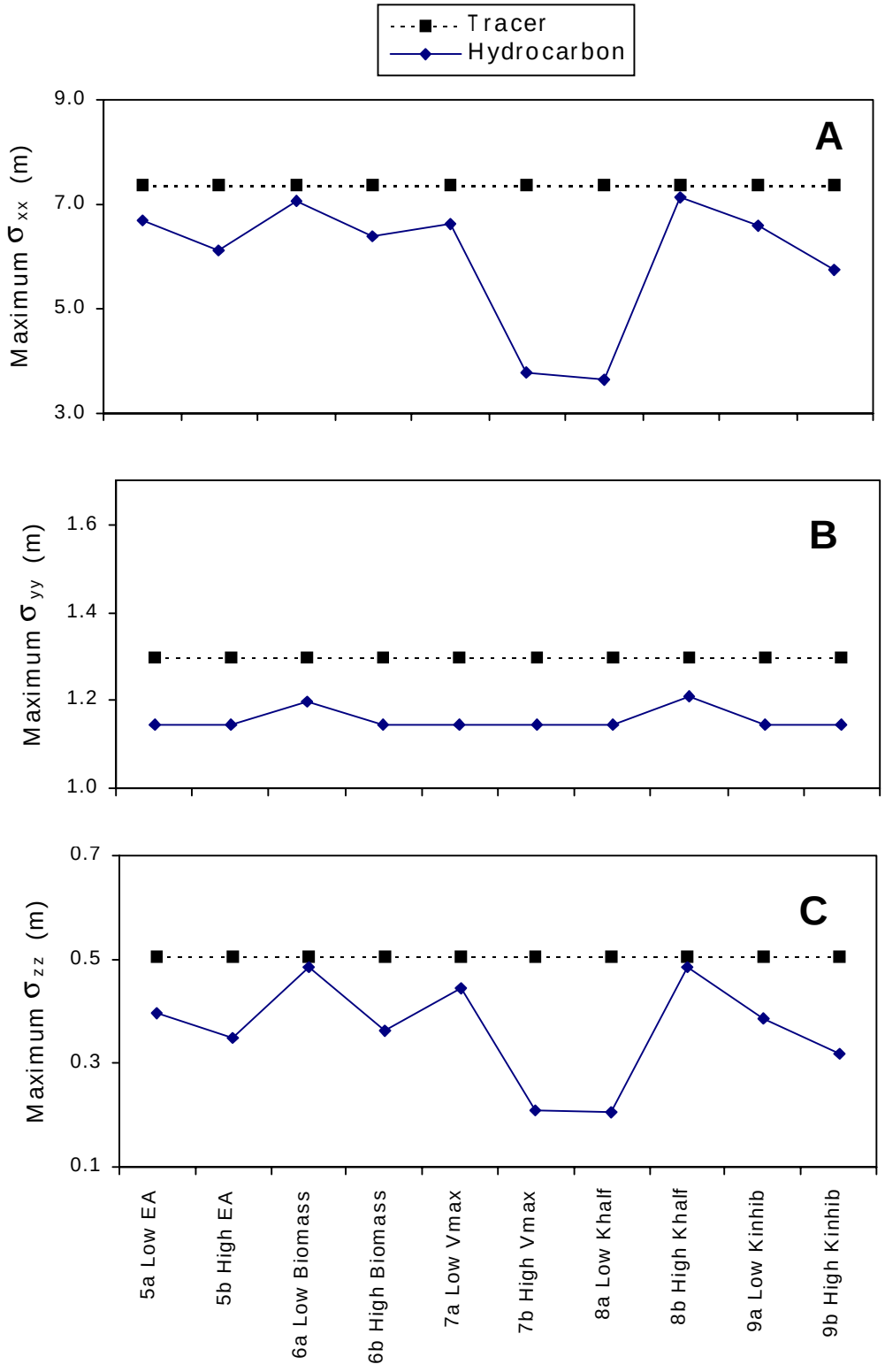

Figure 5.26. Maximum values of the spatial standard deviations (σ_{ii}) of the solute plumes in the x-direction (A), the y-direction (B), and the z-direction (C) for Cases 5 through 9.

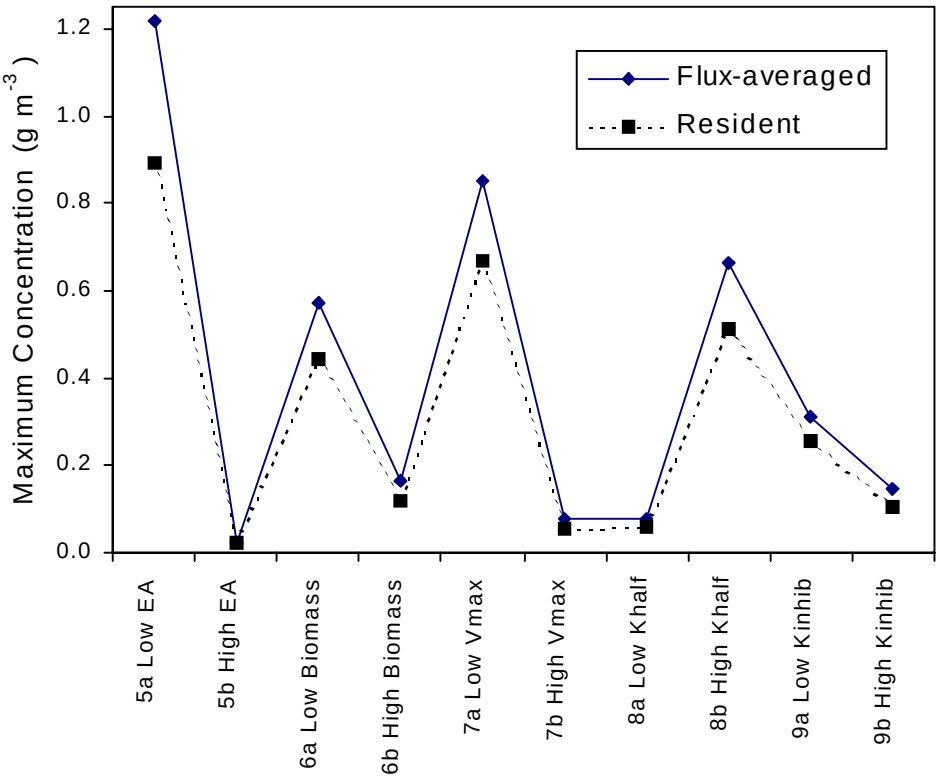

Figure 5.27. Maximum values of the resident and flux-averaged concentrations of hydrocarbon for Cases 5 through 9.

5.7 Conclusions

In all cases, the biodegradation process leads to reduced plume concentrations, mass, and spreading in all directions; i.e., the hydrocarbon plumes were smaller than the conservative tracer plumes. When the available electron acceptor (EA) concentrations were small compared to the hydrocarbon concentration, the rate of hydrocarbon mass loss increased with time as hydrocarbon dispersed over larger areas of the domain and had greater access to EA. Thus, the hydrocarbon loss curve was concave down, which is the opposite of a first order decay model, where the rate of mass loss is directly proportional to the hydrocarbon concentration, and the loss curve is concave up. These results suggest that first order decay models should not be used to simulate biodegradation when EA availability is low.

The spatial moments analysis allowed calculation of the average, large scale movements of the solute plumes, and the average mobility of a plume was inferred from time changes in the location of its center of mass. For these simulations, an increase in soil variability, as expressed by the standard deviation of the horizontal hydraulic conductivity field ($\sigma_{\ln K_h}$), was shown to increase the mobility of a tracer plume, while decreasing the mobility of a biodegradable plume. Decreased mobility was attributed to greater mixing of the hydrocarbon with EA for biodegradation in high $\sigma_{\ln K_h}$ soil. Thus, a biodegradable plume may show fundamentally different behavior in heterogeneous soils compared to a tracer plume. When a homogeneous flow field is used to simulate solute transport, a single field scale value for the dispersivity may not be appropriate for both biodegradable and conservative species. This result is in basic agreement with MacQuarrie and Sudicky (1990), who conclude that it may not be appropriate to simulate transport of biodegradable compounds using homogeneous flow fields and a large scale dispersivity.

Unless soil properties were generated with an unrealistically low correlation scale, the coefficients of variation (CVs) for the average resident concentrations were significantly lower than those of the flux-averaged concentrations. This indicates that the solute concentrations that flow into a region are likely to be more variable in space than the concentrations that exist in the pore space.

The sensitivity analysis showed that hydrocarbon mass loss and H_2S production were sensitive to changes in initial hydrocarbon and EA concentration. Since hydrocarbon mass loss

due to biodegradation depends on the relative concentrations of hydrocarbon and EA, these concentrations should be measured as accurately as possible when modeling a field situation. Of all the biodegradation model parameters, the large scale plume velocity and spreading were most dependent on the Monod kinetic parameters; i.e., the maximum specific rate of substrate utilization ($\nu^{max}_{x,ls,le}$), the substrate half saturation constant ($K^{s}_{x,ls,le}$), and the EA half saturation constant ($K^{e}_{x,le}$). Model outputs were less sensitive to the inhibition coefficient ($\kappa_{le,li}$), and the initial biomass concentration (M_x), although the value of M_x had a significant influence on the lag period that preceded initiation of sulfate reduction.

Overall, the results of these numerical experiments suggest that subsurface biodegradation occurs most readily when aquifer materials are highly variable (i.e. $\sigma_{\ln K_h}$). This condition maximizes the spreading and mixing between EAs and hydrocarbon such that the concentrations, overall mass, and mobility of the hydrocarbon are reduced. Thus, natural attenuation may be most effective as a remediation strategy when aquifer heterogeneities allow mixing to occur readily.